UiT
THE ARCTIC UNIVERSITY OF NORWAY

FACULTY OF SCIENCE AND TECHNOLOGY

Department of Geology

Depositional environments of the Upper Triassic Snadd Formation on the Loppa High, SW Barents Sea

—

Stian André Johansen

EOM-3901 Master thesis in Energy, Climate and Environment.

June 2016

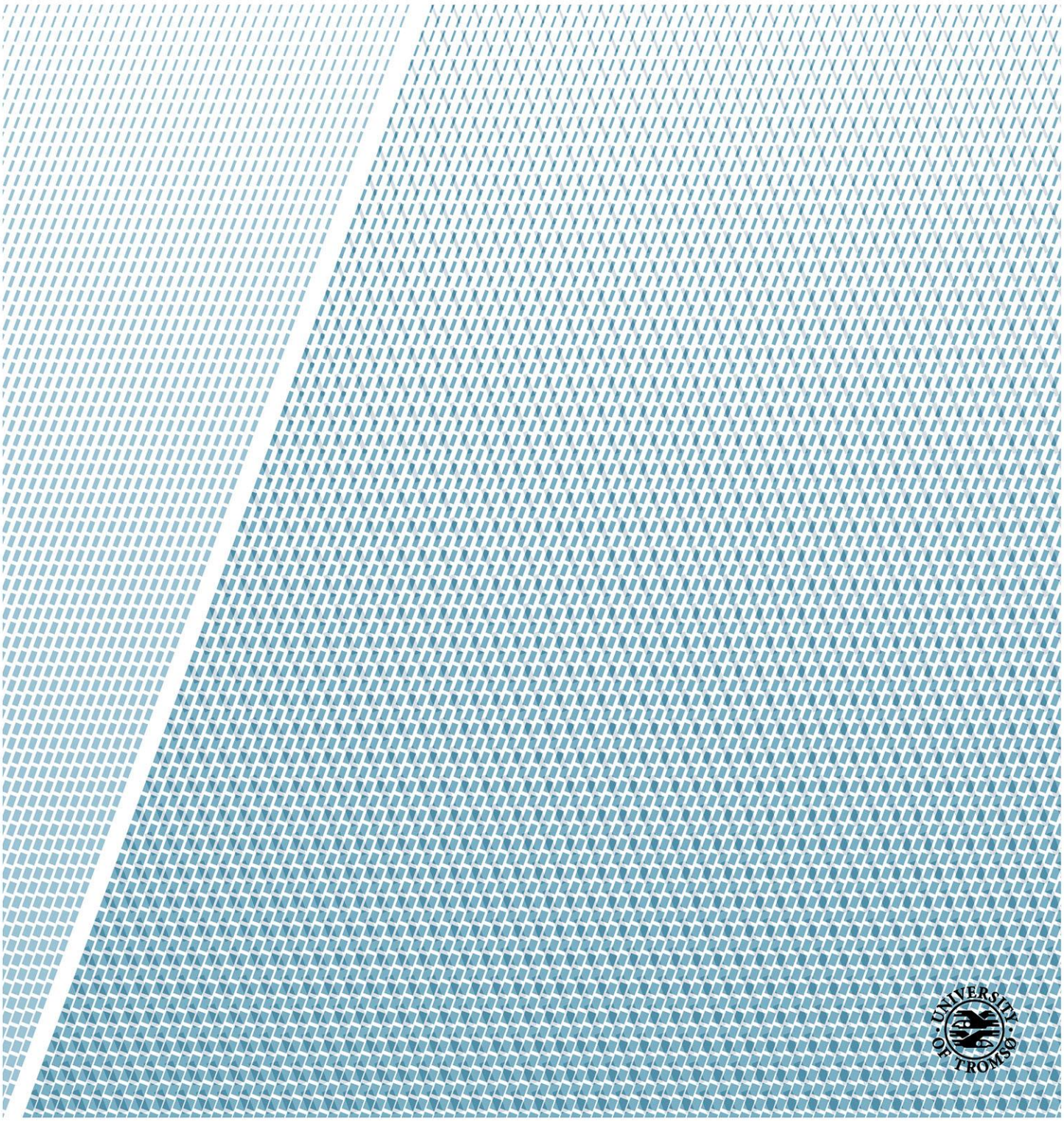

UiT / THE ARCTIC UNIVERSITY OF NORWAY

EOM-3901

Master thesis in Energy, Climate and Environment

Depositional environments of the Upper Triassic Snadd Formation on the Loppa High, SW Barents Sea

Stian André Johansen

June 2016

Faculty of Science and Technology

Department of Geology

University of Tromsø

Abstract

This thesis has focused on the depositional environments of the Upper Triassic Snadd Formation. This formation covers the time-period Ladinian to early Norian with multiple marine regressions and transgressions, resulting in depositional environments ranging from offshore marine shelf to a coastal plain. A 3D seismic dataset and its correlating well have been studied and a refined seismic stratigraphic framework for the Snadd Formation is proposed. The area of investigation is located at the border between the Loppa High, the Bjarmeland Platform and the Hammerfest Basin.

The study defines five time-stratigraphic units within the formation, bounded by regional flooding surfaces. Depositional features observed on seismic data, demonstrate distinct depositional environments within each unit.

This thesis show that a marine setting dominates the lower units (Ladinian to middle Carnian), with three shorter periods of marine regressions exposing the study area to marginal marine and coastal plain processes. In the upper units (middle Carnian to early Norian), a marine regression shifts the dominating environment from marine to a coastal plain. The deposition of the Snadd Formation ends by a marine transgression, known as the early Norian flooding event.

Acknowledgement

5 års studietid, borte på et blunk. Det er tid for å levere inn masteroppgaven. En spennende, men også krevende prosess. Det er mange som fortjener en takk på veien:

Først og fremst må det rettes en stor takk til hovedveileder Tom Arne Rydningen, og biveilederne Iver Martens og Jim Myrvang. Tusen takk for hjelp, både i tide og utide. Det settes stor pris på.

En stor takk må også gå til resten av gjenget på EKM-kullet, ikke bare for faglig hjelp, men først og fremst for et samhold som gjorde skoledagen til en lek. Uten dere hadde jeg nok aldri endt her.

Skal holde meg kortfattet, og noen er sikkert glemt. Uansett, takk.

This research is partially funded by ARCEx partners and the Research Council of Norway (grant number 228107)

Stian A. Johansen

Juni 2016

Table of Contents

1. Introduction and objectives

1.1 Objective

The main objective of this thesis is to describe, analyze and discuss the Snadd Formation on the Loppa High, in order to increase the understanding of this part of the stratigraphy in the southwestern Barents Sea. The aim is achieved using 3D-seismic data supplemented by a correlating wellbore within the survey.

The Snadd Formation covers the Ladinian, Carnian and early Norian of the Late Triassic (approximately 236-215 Ma). Within the formation, depositional environments vary from open marine to paralic, highly affected by several transgressive and regressive events moving the coastline back- and forward over large areas. Distinct internal seismic markers in the formation can represent flooding surfaces, dividing it into seismic subunits.

High-amplitude anomalies are identified on seismic data within paralic intervals of the Snadd Formation. These are easily interpreted to be of a strictly fluvial origin (i.e., fluvial channel sandstones), but as this study will show, they can also represent coastal depositional features such as beach ridges and offshore barrier islands. In order to detect, map and interpret these features and its morphology, it is necessary to use 3D seismic data and geophysical detection methods. This is highly needed in order to understand and possibly reconstruct the varying depositional paleo environment within the seismic formation. The result will contribute to a better understanding of the evolution of this part of the Barents Sea during the Late Triassic.

1.2 Study area

The Barents Sea is located at the wide continental shelf area off the northern coasts of Norway and Russia. Bordered to the deep Atlantic Ocean in the west, the Svalbard archipelago and Franz Josef Land in the north and Novaya Zemlya in the east, covering an area of about 1.3 million km^2. Due to being located on the continental shelf, the Barents Sea is a shallow ocean, with an average water depth of approximately 300 m (Doré, 1995; Smelror et al., 2009).

In 1969, the Norwegian authorities started geophysical investigations in the Barents Sea. Extensive research in the next decade confirmed the existence of thick sedimentary successions and large sedimentary basins, leading to the first well being drilled in 1980 with hydrocarbon discoveries the following year with the Alke and Askeladden gas fields (Doré, 1995).

The study area in this thesis is located southwest in the Barents Sea about 235 km north of Alta, at and around the boundary between the southeastern part of Loppa High, the northwestern part of Hammarfest Basin and the southern part of the Bjarmeland Platform (between 72°05'N, 22°E and 71°55'N, 22°25'E, and 72°10'N, 23°20'E and 72°15'N, 23°E). It covers an area of approximately 850 km^2 at water depths between 300-450 m (Fig. 1.1).

Drilling of the wildcat well 7222/11-1 in 2008 within the study area, led to the Caurus discovery containing both oil and gas. Evaluation of the discovery concluded it to be sub-commercial. A second well was drilled in 2014 (7222/11-2) on the Langlitinden prospect proving sub-commercial gas resources within Kobbe Formation fluvial reservoirs.

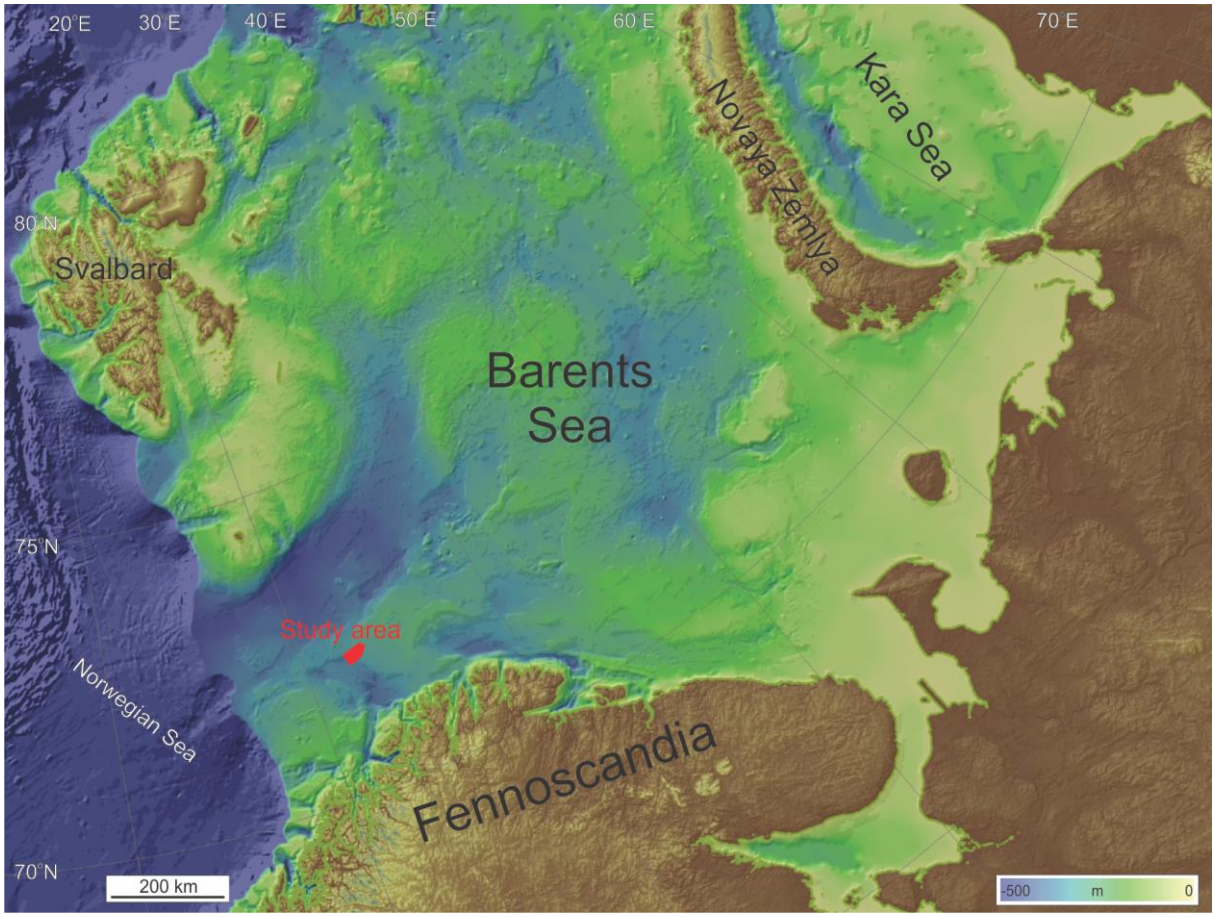

Figure 1.1: Bathymetric map of the Barents Sea with the study area marked in red.

1.3 Seismic stratigraphic techniques and mapping

This study uses the seismic sequence stratigraphic mapping technique in order to identify and understand the paleo-depositional variations. Seismic sequence stratigraphic mapping divides formations into first-, second- and third order units in order to fully understand the changes in the paleo-depositional environment. These changes is represented by boundaries or changes in the reflection configuration within the seismic section (Fig. 1.2). Identifying and mapping these sub-units makes it possible to interpret the paleoenvironment, based on reflection parameters and its associated well logs. Reflection parameters taken into consideration in this study includes reflection amplitude, reflection continuity and geometry of the reflector compared to its surroundings.

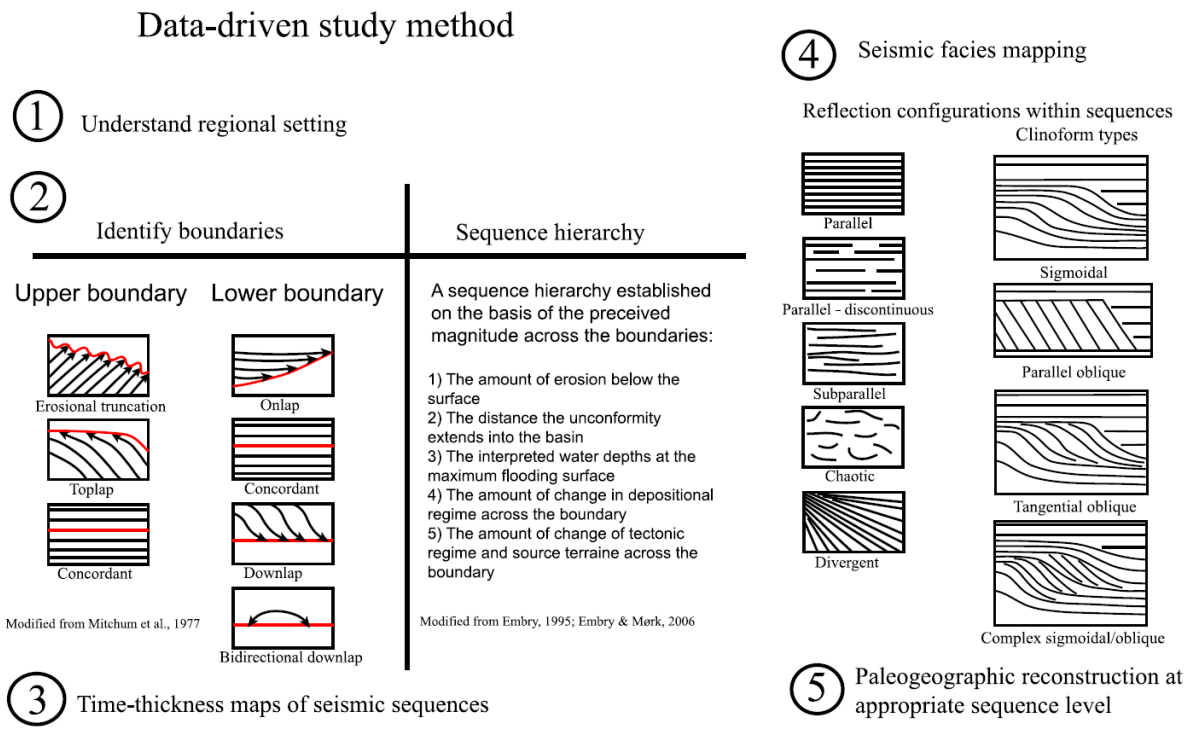

Figure 1.2: The data-driven study method. From Glørstad-Clark et al. (2010), based on the methods of Badley (1985).

1.4 Depositional environments

The depositional environment within the Snadd Formation is recognized to vary from offshore marine, through shelf and shallow marine, to paralic and and fluvial (Glørstad-Clark et al., 2010; Klausen et al., 2015)

By studying changes within seismic, well logs and cores, discrete variations can be mapped in order to fully understand the geologic and environmental development. Klausen et al., (2015) divides the depositional environment into five distinct seismic facies, shown in Figure 1.3. Flooding surfaces (FS) marks periods of marine inundation, where shallow to non-marine depositions are unconformably overlaid by offshore marine deposits (Glørstad-Clark et al., 2010; Klausen et al., 2015). These surfaces have been used to divide the formation into stratigraphic units.

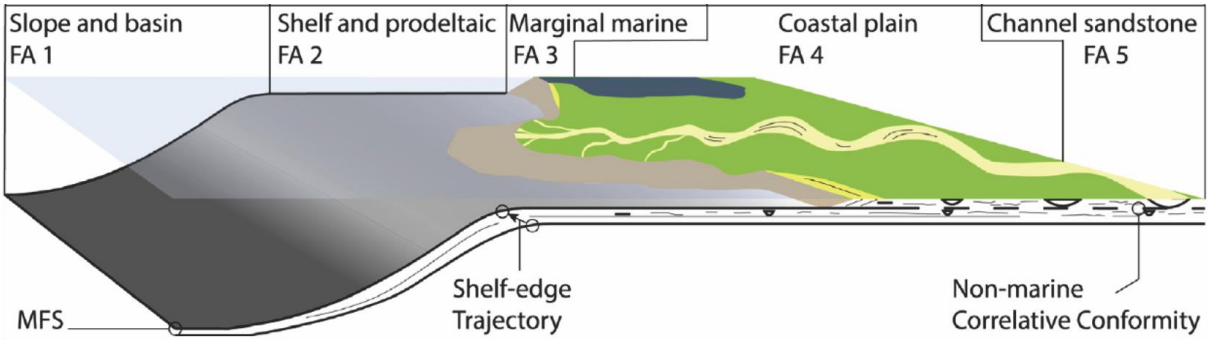

Figure 1.3: The different marine and coastal depositional environments found within the Snadd Formation. Modified from Klausen et al., (2015).

1.4.1 Facies association 1: Slope and basin

Seismic reflectors with a basinwards dip and a clinoform configuration characterize the depositional environment. The height of the clinoforms range between 100 to 500 m, and they have a sigmoidal to oblique shape with a tangential bottomset. The clinoforms represent the marine shelf edge and slope, usually dominated by parallel mud depositions (Sollid et al., 2004; Klausen et al., 2015).

1.4.2 Facies association 2: Shelf and prodeltaic

Closer to land and higher up in the stratigraphy relative to the previous clinoforms, the area is dominated by parallel, continuous, high-amplitude seismic reflectors. These reflectors are often seen in relationship with flooding surfaces, overlying the FSs

conformably. Its horizontal and lateral extent varies, but usually the thickness is between 20- 100 ms over several kilometers. In outcrops at eastern Svalbard, the facies consist of bioturbated, gray mudstone, interlayered by minor sand deposits between 0,5-1,5 m with wave ripple lamination and hummocky cross stratification (Sollid et al., 2004; Klausen et al., 2015).

1.4.3 Facies association 3: Marginal marine and shoreface (coastal)

The seismic facies is characterized by alternating high- and low-amplitude, parallel seismic reflectors, with low to moderate continuity. The facies is about 20-40 ms thick, possibly hundreds of kilometers parallel to the depositional strike and 1-10 km normal to it. The high amplitude features in the reflectors appear as straight and elongated in horizontal seismic section. In well logs the environment is characterized by a discrete coarsening upwards trend, shown as a gradual decrease in gamma ray values (Sollid et al., 2004; Klausen et al., 2015).

1.4.4 Facies association 4: Coastal plain

The coastal plain facies is characterized by irregular, discontinuous and weak to moderate seismic reflectors. The facies could be between 30 and 500 meters thick, laterally spreading over hundreds of kilometers. The coastal plain facies is often laying conformable on top of the marginal marine facies, but is sometimes interrupted by an overlying, unconformable marine shelf facies. In well logs, its serrated shape is often typical to the coastal plain environment. The environment is highly influenced by heterolithic, fluvial elements of deposition (Sollid et al., 2004; Klausen et al., 2015).

1.4.5 Facies association 5: Channel sandstone bodies

The facies of channel sandstone bodies is characterized by a strong, discontinuous amplitude with varying values. In plan-form they usually have a sinuous to straight shape, with varying lengths up to tens of kilometers and somewhat smaller widths. The channel sandstone bodies are found in relation with coastal plains. The channels are recognized in seismic sections by the erosive base with infill reflectors discontinuous to the surroundings (Sollid et al., 2004; Klausen et al., 2015).

2. Geological background

2.1 Tectonic development

The greater Barents Sea can be divided into two large and different geological provinces, separated by an extensive monoclinal structure located in the center with an orientation from north to south. The eastern province was mainly influenced by the tectonical history of Novaya Zemlya, Timian Pechora Basin and the Uralian Orogeny, while post-Caledonian rifting, as well as some later rifting episodes leading to the continental breakup of the Eurasian plate along the northwestern margin mainly affected the western province (Smelror et al., 2009).

As this thesis focus on the southwestern part of the Barents Sea, the eastern province will not be further described.

2.1.1 Paleozoic

The Caledonian orogeny culminated about 400 Ma resulting in the consolidation of the Laurentian and Baltican plates into the Laurasian continent, and thereby the closing of the Iapetus Ocean (Smelror et al., 2009). After the compressional regime followed an era of extension, with a structural trend varying between N-S in the western Barents margin, and NE-SW trend at the southwestern Barents Sea. Following, during Devonian to Early Carboniferous, the Caledonian orogeny was eroded and the accumulated sediments deposited in the western Barents Sea (Worsley, 2008; Smelror et al., 2009).

The Carboniferous was dominated by an extensional regime in the western Barents Sea, as Svalbard moved further northwards to its present day location. This created huge rift structures possible to recognize on seismic data below Upper Carboniferous to Lower Permian (Worsley, 2008; Smelror et al., 2009). The northern movement also created a change in climate, which together with a regional transgression formed large carbonate platforms deposited with thick evaporitic successions in the southwestern parts of the shelf, including the Tromsø Basin, the Bjørnøya Basin, and the Nordkapp Basin (Worsley, 2008).

2.1.2 Mesozoic

Triassic was a tectonically quiet period in the Western Barents Sea, with regional subsidence and high sedimentation rates with the sediment source being the Urals in the southeast, the Norwegian Caledonides and the Baltic craton to the south and the North American craton to the west, with the sediments being transported to the Finnmark Platform, the Hammerfest Basin and the Nordkapp Basin (Smelror et al., 2009). Though tectonically quiet, Loppa High was uplifted and eroded due to rifting west of the high, indicated by a thickening of the Bjørnøya Basin. There is also minor rifts found on the Bjarmeland and Finnmark Platforms (Smelror et al., 2009; Glørstad-Clark et al., 2010; Klausen et al., 2015).

During Late Triassic-Early Jurassic, large areas of the Barents Sea were uplifted and eroded. This led to a change of depositional environment in later Early Jurassic (early Toarcian) from flood plain to westward prograding coastal settings. In the westernmost basins, during late Toarcian, the depositional environment is of a shallow marine origin. The Barents Sea regression reached its maximum in the Middle Jurassic, leading to large parts of the shelf being exposed to erosion. Because of this, there is a big depositional gap in large areas at the western Barents Sea. From regression- maximum in Middle Jurassic, the sea level changed to a transgressional maximum. Erosion still occurred at the Loppa and Stappen Highs, as their uplift continued due to the Cimmerian movements (Smelror et al., 2009; Glørstad-Clark et al., 2010).

At the end of Jurassic a period of overall regression started, continuing into Early Cretaceous. As the Amerasian Basin in the Arctic Ocean opened, this created a rift system with some tilting, and uplift in the northern parts of the Barents Sea. Because of this, increased amounts of sediments were transported from the north to the rapid subsided and deep lying western Harstad, Tromsø and Bjørnøya basins, resulting in an estimated 5-6 km shaly sequence (Faleide et al., 1993; Doré, 1995; Smelror et al., 2009). Late Cretaceous followed the earlier trend, with subsidence in western basins, while uplift took place in the east. A continental breakup along the North Atlantic rift created a major dextral stress field along the Senja-Hornsund lineament. This lineament acted as a relay zone between the spreading ridges during the Paleogene (Faleide et al., 1993; Smelror et al., 2009).

2.1.3 Cenozoic

During the transition between Paleocene and Eocene time, the Norwegian-Greenland Sea expanded forming a sheared western Barents Sea margin that in Eocene time experienced both transtentional and transpressional deformation. This caused faulting and uplifting in the southern Sørvestnaget Basin, while the northern part experienced extensional faulting as a result of tectonic and magmatic activity in the Vestbakken Volcanic Province (Faleide et al., 1993).

In Oligocene the Eocene faults and volcanic activity at Vestbakken Volcanic Province were reactivated due to a change in the relative plate motion. Later in Oligocene the margin became tectonically quiet, making the post-Oligocene sedimentary deposits at and nearby the western margin mostly of glacial origin. (Faleide et al., 1993; Smelror et al., 2009)

2.2 Stratigraphy and depositional environments

The stratigraphy in the western Barents Sea range from Late Paleozoic to Quaternary (Fig. 2.3). Available information about the underlying basement is limited, but indirect evidence implies that it was consolidated during the Caledonian orogeny (Gudlaugsson et al., 1998; Worsley, 2008; Glørstad-Clark et al., 2010).

2.2.1 Paleozoic

During Upper Paleozoic most of the Barents Sea experienced crustal extension, creating massive rifting structures. Alluvial fans with a NE-SW trend acted as infill in the rifted basins during Late Devonian to Early Carboniferous, depositing large amounts of continental clastics with a coarsening upwards trend both in rifts and on floodplains (Billefjorden Group) (Worsley, 2008).

This was followed by an establishment of an extensive carbonate platform created in the latest Carboniferous throughout Early Permian together with evaporitic deposits in local basins (Gipsdalen Group) (Worsley, 2008; Smelror et al., 2009; Glørstad-Clark et al., 2010). During Permian the oceanic climate shifted from shallow warm waters to temperate, changing the biogenic composition to cool water carbonates (Bjarmeland Group). Late Permian experienced another decrease in water temperature, changing the regime to silica-rich fine clastics (Tempelfjorden Group) (Worsley, 2008).

2.2.2 Mesozoic

A change from silica-rich shale to non-siliceous shales mark the shift from Late Permian to Early Triassic, a transition still poorly understood due to a significant hiatus on highs and platforms especially, during the latest Permian (Worsley, 2008). This non-siliceous shale stratas are named the Sessendalen Group, including the Havert and Kobbe Formations, a group that range between less than 100 m at pre-existing structural highs to more than 1500 m at the southwestern continental shelf. The deposition during Triassic is massively influenced by sediments eroded and transported from firstly the Baltic Shield and later the Urals, creating a northwesterly prograding coastline (Worsley, 2008; Glørstad-Clark et al., 2010).

During Ladinian a northwestern prograding system developed, establishing deltaic and floodplain environments, depositing fine grained clastics at the southwestern Barents Shelf (Fig. 2.1 & 2.2). Through Carnian the subsidence and sedimentation continued with high, but decreasing rates from the Baltic Shield, resulting in a relatively thick and widespread non-marine sedimentary package (Storfjorden subgroup/Snadd Formation) (Worsley, 2008; Glørstad-Clark et al., 2010; Klausen et al., 2015).

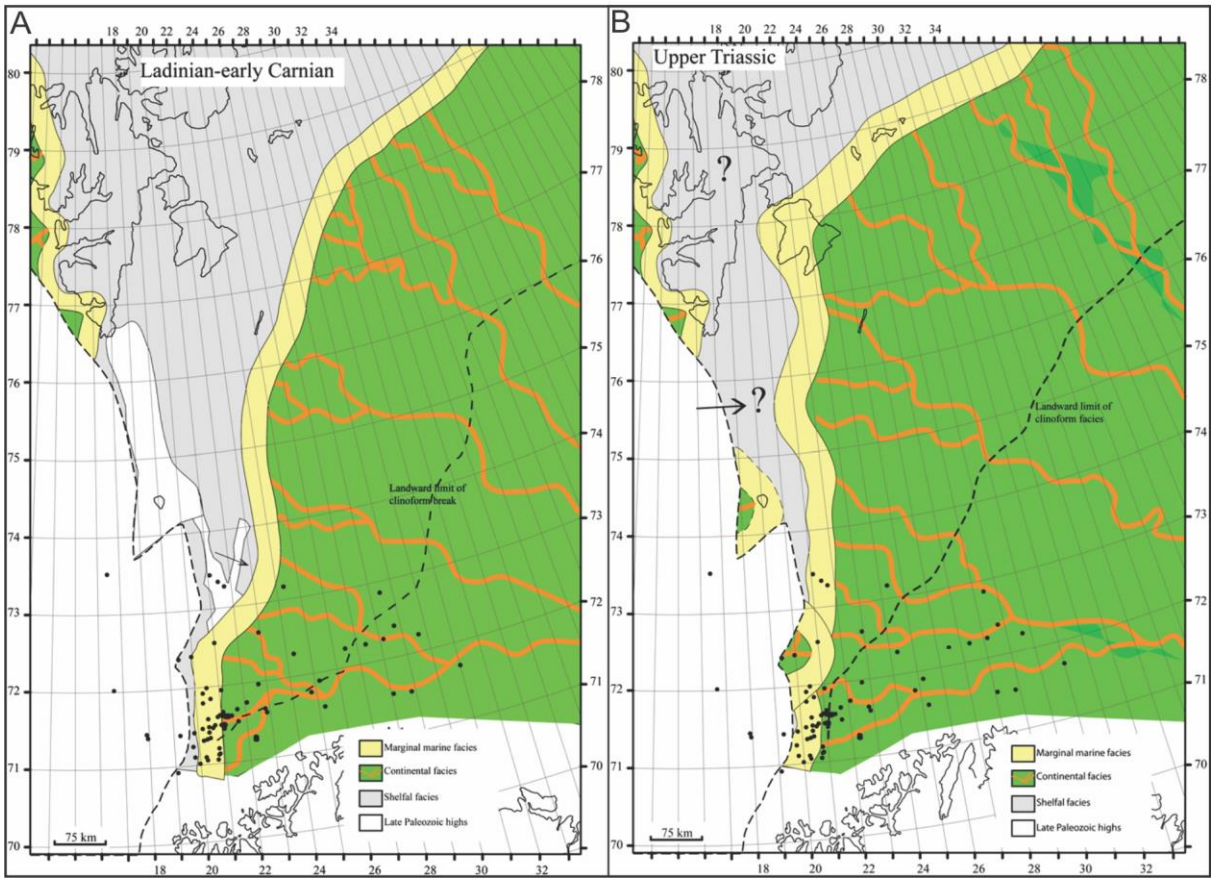

Figure 2.1: ***A:*** *Paleogeographic reconstruction by Glørstad-Clark et al., (2010) of Ladinian to early Carnian time.* ***B:*** *Paleogeographic reconstruction by Glørstad-Clark et al., (2010) of Upper Triassic time. Figure modified from Glørstad-Clark et al., (2010).*

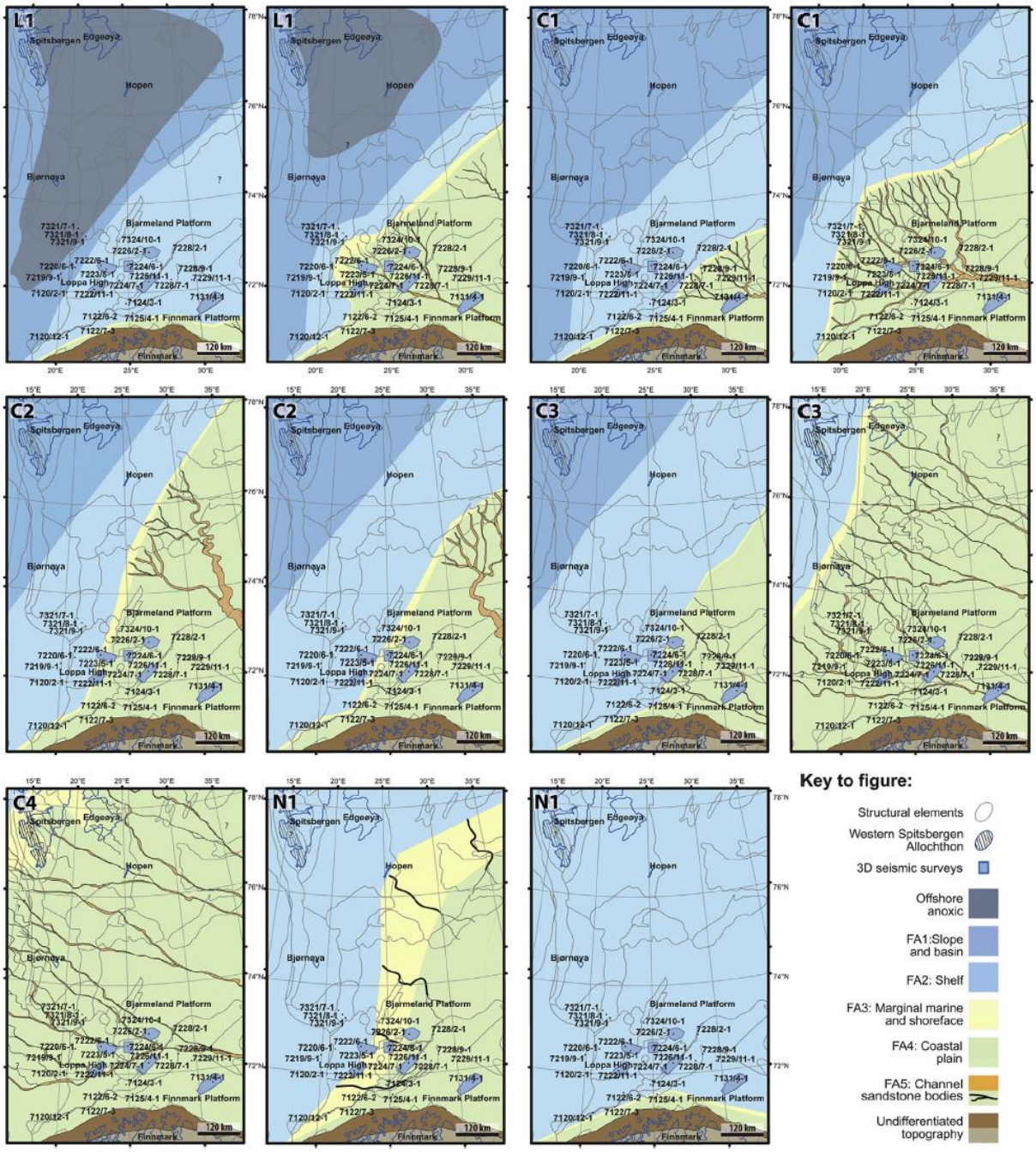

Figure 2.2: Paleogeographic reconstruction by Klausen et al., (2015) during Ladinian to early Norian, the time of Snadd Formation deposition. Figure from Klausen et al., (2015).

A regional relative sea-level rise in late Norian to Rahetian established a marine regime, depositing fine grained clastics capping the deltaic Snadd Formation (Fig. 2.2). The sequence is called the Fruholmen Formation (Klausen et al., 2015).

Late Jurassic to Early Cretaceous tectonics created subsidence along the western margin, with the result of an extremely large sandstone succession deposited during Cretaceous along the down dipping flank of Loppa High towards the Hammerfest Basin (Smelror et

al., 2009). In Late Cretaceous a marine transgression created a shelf environment, resulting in deposition of the Kveite and Kviting Formations (Worsley, 2008).

2.2.3 Cenozoic

Another major transgression occurred in early Paleocene, creating a marine shelf environment depositing fine clastics and carbonates (Sotbakken Group) (Worsley, 2008; Glørstad-Clark et al., 2010).

During Neogene repeated glaciations with correlated subcidence/uplift and erosion created large wedges over and off the continental shelf margins, redepositing eroded sediments at the continental slope (Vorren et al., 1991; Faleide et al., 1996; Worsley, 2008; Glørstad-Clark et al., 2010; Laberg et al., 2012).

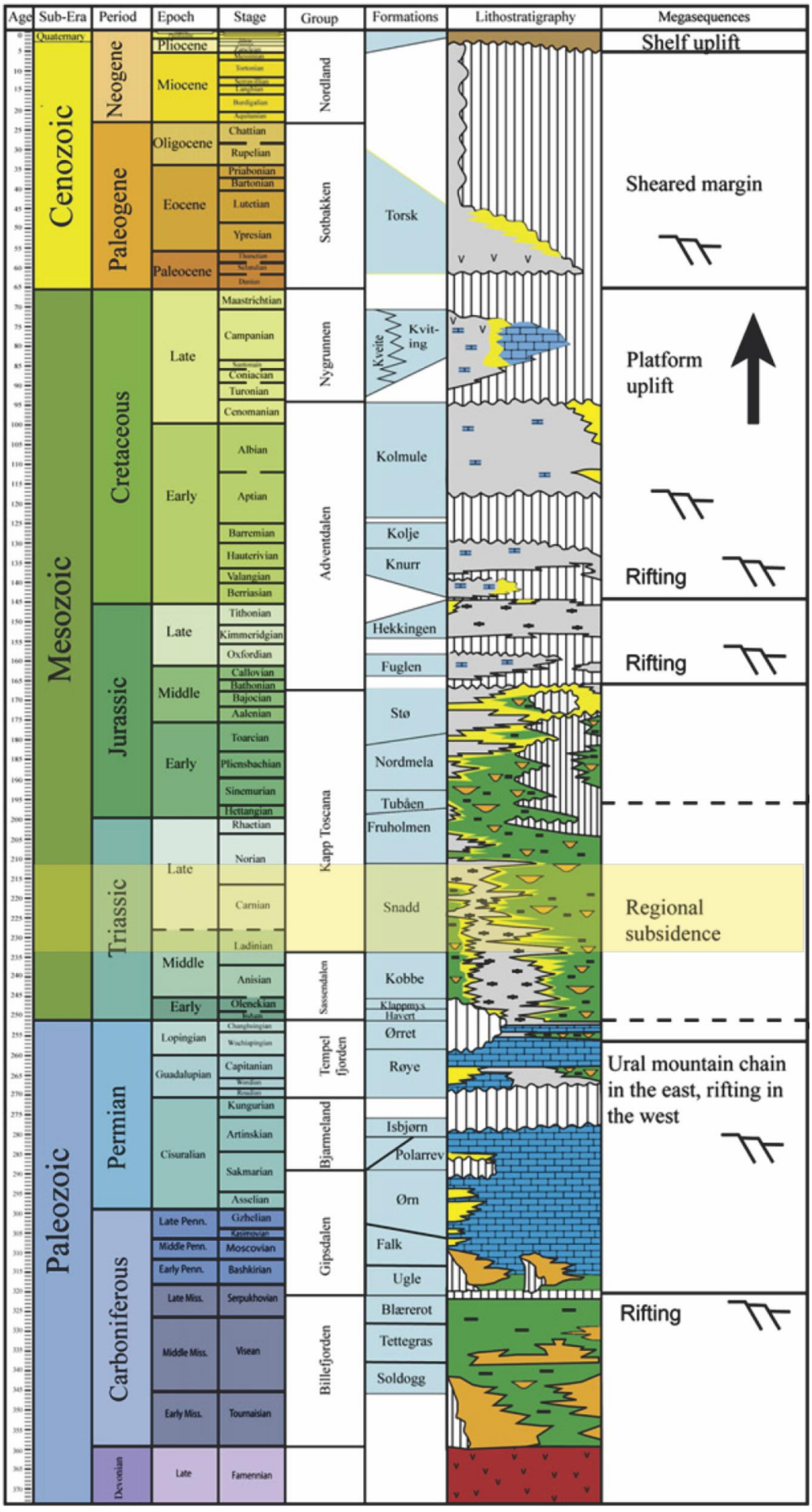

Figure 2.3: Lithostratigraphic diagram of the western Barents Sea. The Snadd Formation highlighted in yellow. Figure modified from Glørstad-Clark et al., (2010)

2.3 Structural setting

2.3.1 Loppa High

The western part of the dataset used in this thesis is at the Loppa High, a high named after an island and a district at the coast of Finnmark. It incorporates the Polheim Platform in the west, and is located between 71°50'N, 20°E and 71°55'N, 22°40'E, and 72°55'N, 24°10'E and 73°20'N, 23°E with a diamond shaped outline (Gabrielsen et al., 1990), bordered to the Hammerfest Basin in the south-southeast, and the Bjørnøya Basin in the northwest (Fig. 2.4). It consists of an eastern platform, and a crestal western and northwestern margin. In the south it is bounded by the Asterias Fault Complex, in the west by the Ringvasøy-Loppa and the Bjørnøyrenna Fault Complex, and in southeast by a monocline towards the Hammerfest Basin and the Bjarmeland Platform. The northeastern limit of the high is marked by a large salt structure called the Svalis Dome, and its associated syncline called the Maud Basin (Gabrielsen et al., 1990).

Loppa High has its genesis at Late Permian to Early Triassic, in a diverging tectonic regime creating uplift of the high. Due to tectonism, the uplift of Loppa High have been reactivated in both Late Jurassic- Early Cretaceous and Late Cretaceous- Cenozoic (Gabrielsen et al., 1990). Because of the Loppa High setting, being exposed to multiple uplifts, the metamorphic basement lays at relatively shallow depths (especially in the west), making it highly associated with a positive gravity and magnetic anomaly (Gabrielsen et al., 1990).

2.3.2 Bjarmeland Platform

The Bjarmeland platform represents a stable area between the Hammerfest and Nordkapp Basins in the south and southeast, Sentralbanken and Gardarbanken Highs in the north, and the Loppa High and the Fingerdjupet Basin in the west (Fig. 2.4). The platform includes many domes, among them the Samson Dome located about 50 km northeast of the study area. The platform sediments dip gently to the south because of an regional uplift during tertiary. Still, the platform represent a structural element that has been relatively stable since Late Paleozoic (Gabrielsen et al., 1990).

The Bjarmeland Platform started to develop as a stable platform during Late Carboniferous, and is assumed underlain by Palaeozoic and Precambrian rocks. In Early Triassic the platform was terminated to the west by a north-south orientated fault zone,

while Late Mesozoic and Tertiary tectonism gave rise to the Loppa High (Gabrielsen et al., 1990).

2.3.3 Hammerfest Basin

South of the Loppa High and the Bjarmeland Platform, separated by the Asterias Fault Complex, is the Hammerfest Basin (Fig. 2.4). It is limited by the Finnmark platform in the south, and by the Tromsø Basin in the west. The Hammerfest Basin has a general westwards dip towards the Tromsø Basin (Gabrielsen et al., 1990).

The structural predecessors containing the large NE-SW trending basins of the southern Barents sea, including the Hammerfest Basin, can be dated back at Late Devonian to Early Carboniferous times. Separation between the Hammerfest Basin and Finnmark Platform took place in Late Carboniferous, and the outline of todays Hammerfest Basin emerged during Mid Jurassic (Gabrielsen et al., 1990).

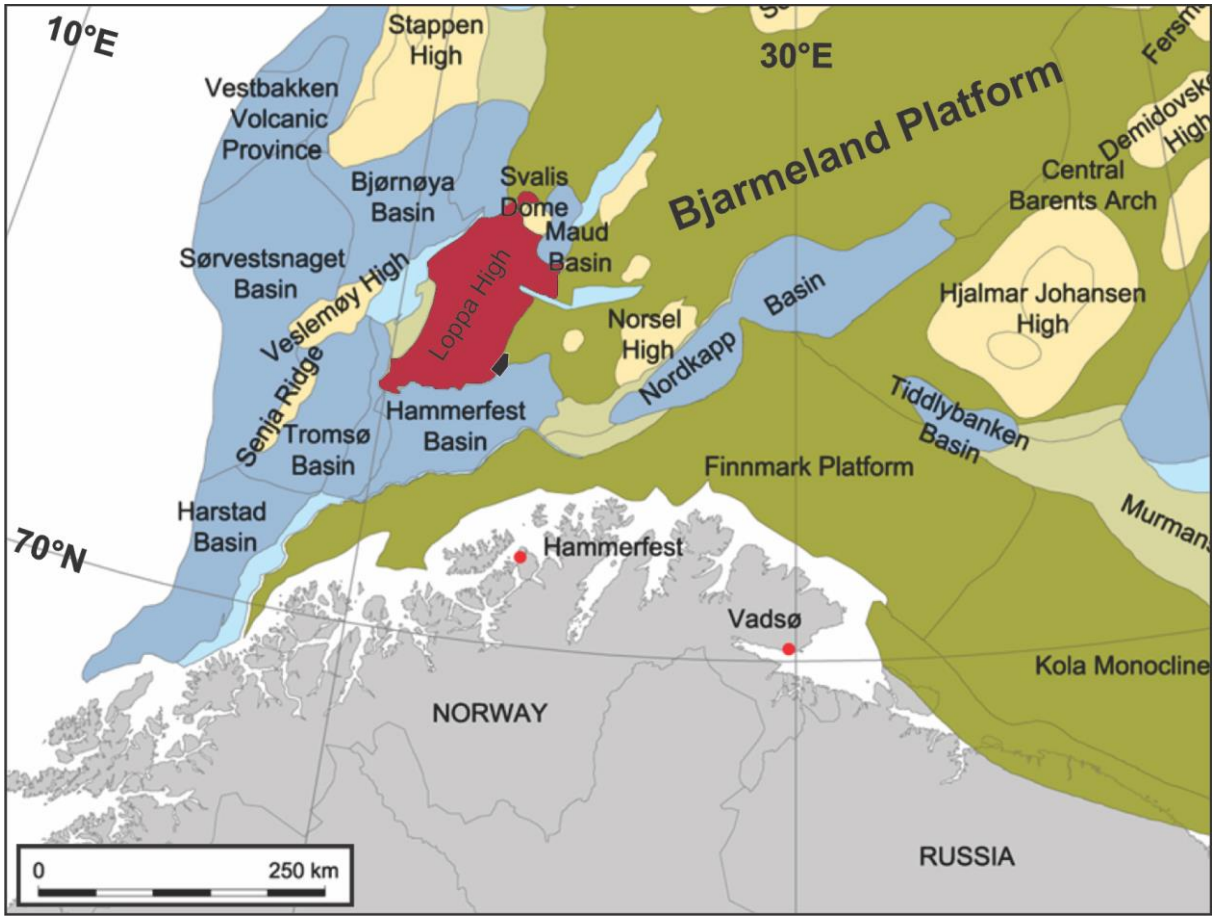

Figure 2.4: Overview of the main structural elements in the southwestern Barents Sea. The main structural element in this study, the Loppa High, is highlighted in red, while the 3D dataset is marked in black. Figure modified from Henriksen et al. (2011).

2.4 Seismic stratigraphy of the Upper Triassic Snadd Formation

Numerous studies have focused on the Triassic succession (Fig. 2.5) in the Barents Sea (Dalland et al., 1988; Johansen et al., 1993; van Veen et al., 1993; Skjold et al., 1998; Mørk and Elvebakk, 1999; Bugge et al., 2002; Bullimore et al., 2004; Glørstad-Clark et al., 2010, 2011; Henriksen et al., 2011a, 2011b), but the Upper Triassic Snadd Formation is less studied (Dalland et al., 1988; Mørk et al., 1999; Klausen et al., 2015).

The Snadd Formation is a part of the Upper Triassic sedimentary succession (Fig. 2.5), deposited in relatively a quiet tectonic period. A relatively thick and widespread sedimentary package of non-marine origin characterize the formation, containing large river deposits with hydrocarbon potential (Klausen et al., 2015). Variations in both sediment source area and shoreline position create widespread changes in depositional elements. The depositional environments both above and below (Fruholmen and Kobbe Formations) are on the other hand characterized by an open marine setting (Klausen et al., 2015). These boundaries are both marked by regional flooding surfaces traceable in the seismic section.

The depositional environment within the Snadd Formation range from offshore marine in the lower part through coastal (paralic) to a more continental dominated setting in the upper part. Within the formation, periods of marine inundation have occurred, creating flooding surfaces with marine deposits overlying shallow or non-marine sediments. These surfaces are used to divide the formation into stratigraphic sub-levels.

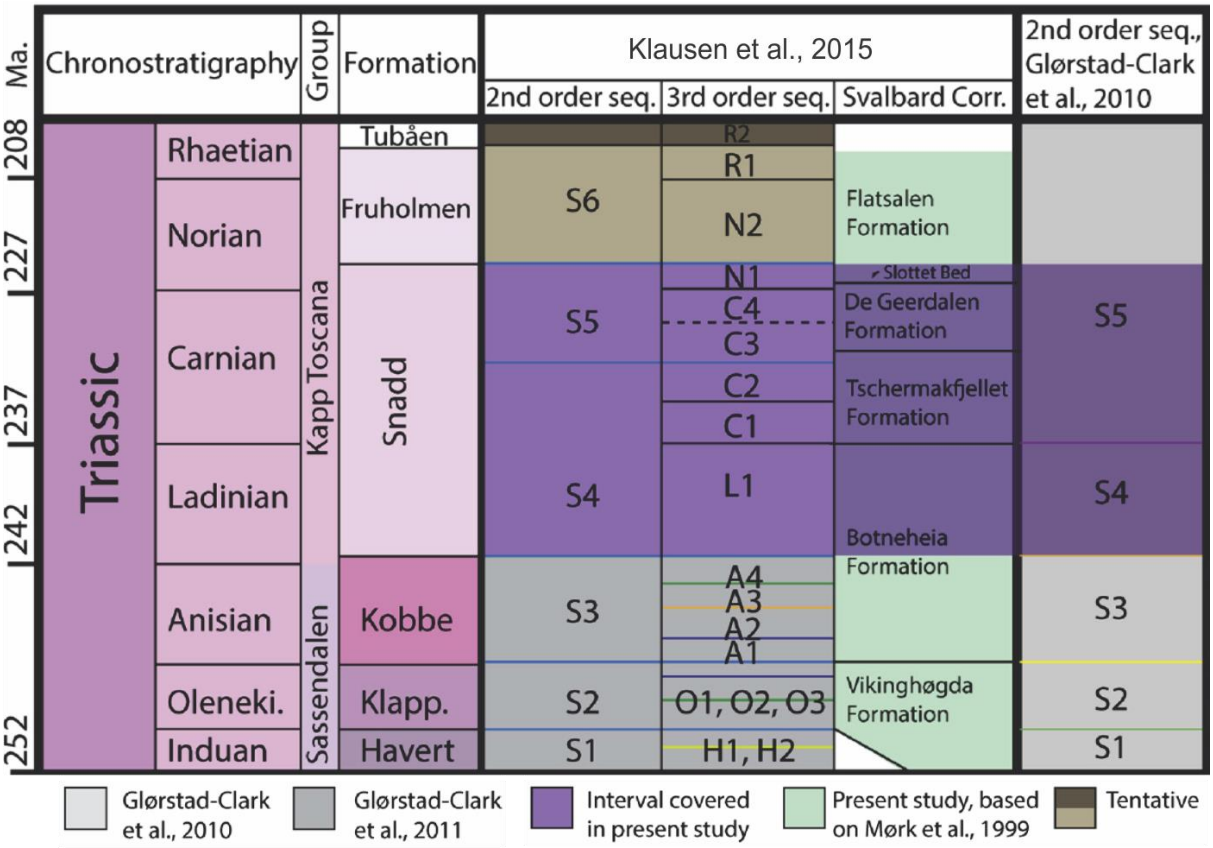

Figure 2.5: Lithostratigraphic diagram of the Triassic sequence in the western Barents Sea with second- and third-order units interpreted by Klausen et al., (2015). Figure modified from Klausen et al., (2015)

3. Data & Method

3.1 Dataset

This study uses the 3D seismic data set SG9803 located at the boundary between the Loppa High, the Hammerfest Basin and the Bjarmeland Platform (Fig. 3.1), covering an area of approximately 850 km^2.

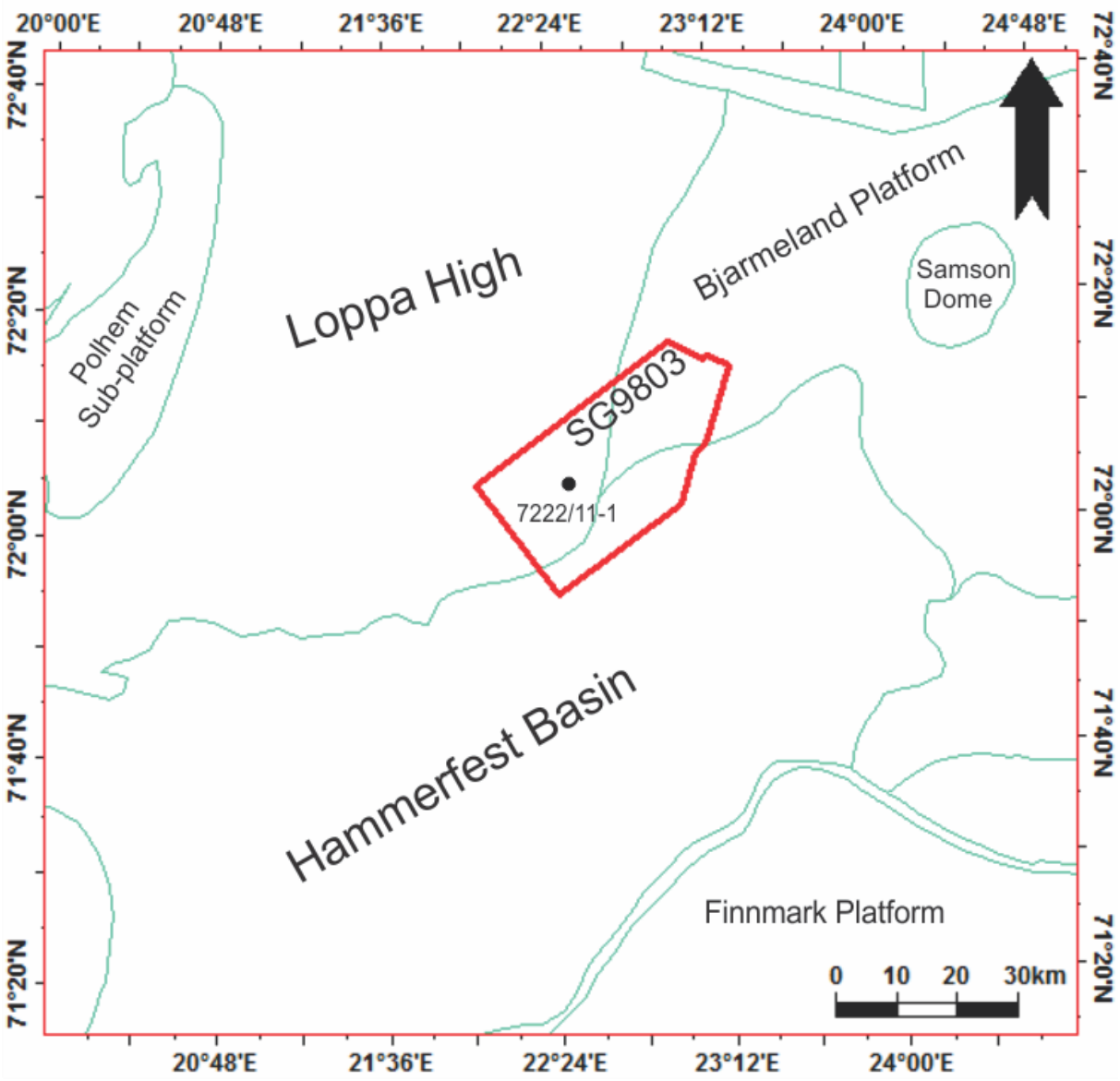

Figure 3.1: Location of the 3D dataset (red polygon) and the correlated well (black point). Main structural elements in and around the study area marked as green lines.

3.1.1 3D-seismic survey

The 3D-seismic dataset SG9803 was gathered by Saga Petroleum in 1998. The dataset covers a total area of approximately 850 km^2, with an inline direction from northeast to southwest. An analyze of the seafloor reflector show that, using the SEG polarity standard from Sheriff (2006), the survey use a zero-phase signal with a normal polarity. The distance between each trace is 12,5 m (Fig. 3.2).

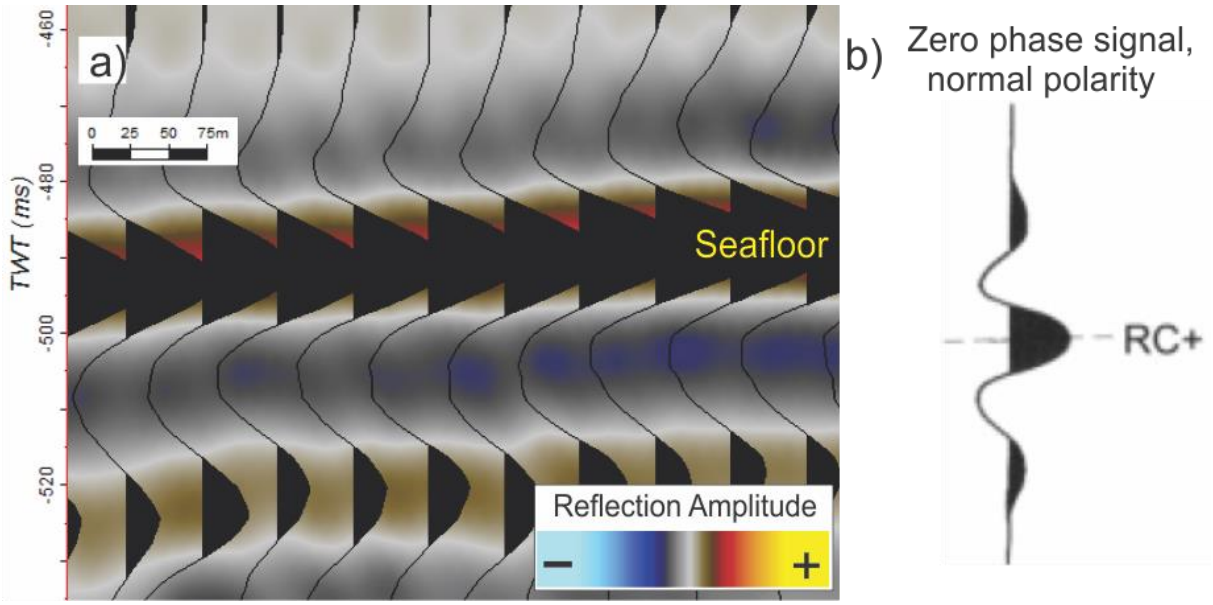

Figure 3.2: a) Seismic intersection showing the seafloor wiggle reflection in the 3D seismic survey. b) Model of the seismic trace, a zero phase signal with normal polarity using the SEG polarity standard from Sheriff (2006), the same model as the trace of the 3D seismic dataset in this study.

3.1.2 Well data

The extent of the Snadd Formation in the seismic survey have been correlated and interpreted using the stratigraphic boundaries of well tops (NPD, 2016) in the exploration well 7222/11-1. The well was a wildcat exploration well drilled at autumn 2008 by StatoilHydro resulting in the Caurus discovery, an oil and gas discovery found too small for profitable development (NPD, 2016).

3.2 Seismic reflection theory

Seismic reflection is a basic technique, and the most important tool used to explore and map subsurface structures in detail. The technique is preformed by sending seismic waves into the ground, and the seismic waves is reflected in the subsurface. As it arrives back at the surface the arrival time is recorded, and by using this information it is possible to map the subsurface and its variations. The subsurface reflection is caused by interfaces in the rocks (called reflectors), that partly reflects the waves due to differences in acoustic impedance (Equation 3.1) between the upper and lower reflectors. The amount of energy reflected at a seismic reflector is determined by the weight of change in acoustic impedance between the sedimentary layers, and is calculated as the reflection coefficient (Equation 3.2). This creates seismic lines that unveils underground sedimentary structures. (Andreassen, 2009)

$$Z = \rho V \tag{3.1}$$

Equation 3.1: A seismic layers Z = acoustic impedance equals its ρ = density (kg/m^3) multiplied by its acoustic V = velocity (m/s).

$$R = \frac{(Z_2 - Z_1)}{(Z_2 + Z_1)} = \frac{\rho_2 V_2 - \rho_1 V_1}{\rho_2 V_2 + \rho_1 V_1} \tag{3.2}$$

Equation 3.2: The strength of the seismic reflection is created by the change in acoustic impedance between two seismic layers is calculated as the reflection coefficient (R). Z_1, ρ_1 and V_1 is respectively the acoustic impedance, density and acoustic velocity of the upper sedimentary layer, while Z_2, ρ_2 and V_2 is acoustic impedance, density and acoustic velocity respectively of the lower sedimentary layer. Following the equation it shows that if $Z_2 > Z_1$ R will be positive, and negative when $Z_1 > Z_2$. If $Z_2 = Z_1$, R will be zero.

3.3 Seismic resolution

Seismic resolution is the limit of the amount of stratigraphic detail possible to extract from seismic data. The aspects of seismic resolution is separated into the horizontal and vertical direction. The ability to distinguish between two individual reflectors is depending on the seismic wavelength (Sheriff, 1985).

$$\lambda = \frac{v}{f} \tag{3.3}$$

Equation 3.3: The relationship between λ= Wavelength (m), v = acoustic velocity (m/s) and f = frequency (Hz)

The seismic resolution decreases with depth, as the wavelength increases (Fig 3.3). With increasing depth the rocks tend to have a higher velocity due to its higher degree of compaction. In addition, the frequency will decrease as higher frequencies attenuates at a faster rate than lower frequencies (Sheriff, 1985).

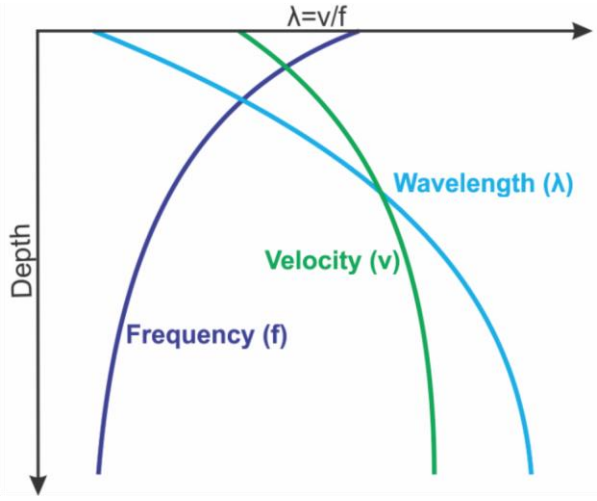

Figure 3.3: The change between the wavelength, velocity and frequency of the seismic signal with increasing depth. Figure modified from Brown (1999).

3.3.1 Vertical resolution

The vertical resolution is defined as the minimum thickness a layer must have in order to be distinguished as a separate layer in a seismic section, and is given as:

$$Vr = \frac{\lambda}{4} \tag{3.4}$$

Equation 3.4: The relationship between the Vr = vertical resolution (m) and the λ = wavelength (m).

When the layer thickness is more than half of a wavelength, the spikes will not interfere and two separate reflections will be produced. As the thickness approaches a quarter wavelength, the reflections will interfere constructively (merging into one reflection with an amplitude increase). At thicknesses lower than a quarter of a wavelength, the reflections will interfere destructively (amplitude decrease, reflectors cancelling each other) until reaching the limit of visibility (λ/30) where a layer below this thickness no longer will be visible (Sheriff, 1985).

With an average acoustic velocity at 3000 m/s and a peak frequency of 29 Hz, the vertical resolution is calculated to be approximately 25 m.

3.3.2 Horizontal resolution

Horizontal resolution is usually described using the Fresnel zone, and is the horizontal distance needed in order to separate two elements from each other (Fig. 3.4). The first Fresnel zone is defined as the area that reflects energy that reaches the detector within half of a cycle. The radius of the Fresnel zone is given as equation 3.5 for unmigrated seismic sections (Sheriff, 1985).

$$rf = \frac{v}{2}\sqrt{\frac{t}{f}} \tag{3.5}$$

Equation 3.5: r f = radius of the Fresnel zone (m), v = Average velocity (m/s), t = Two-way travel time (s), f = Dominant frequency (Hz).

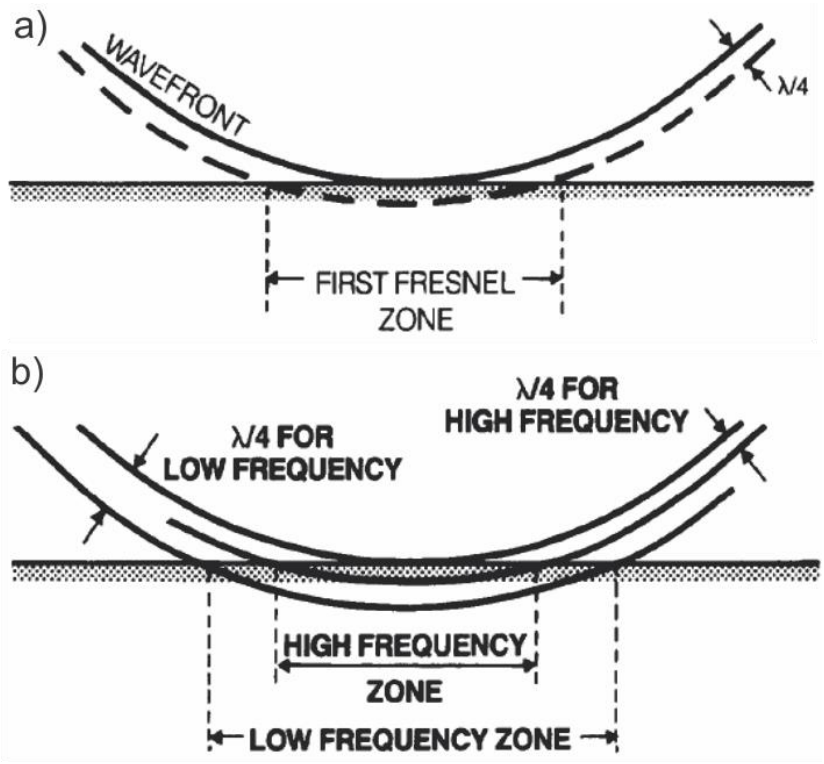

Figure 3.4: a) The first Fresnel zone is defined as, in and around, the point where the reflector is first tangent to the wavefront, limited by the area that the wavefront arrives a quarter of a wavelength later makes with the reflector. b) The Fresnel zone increases with a decreasing frequency. Figure modified from Sheriff (1985)

The horizontal resolution could be significantly improved by migration, shrinking the Fresnel zone (Fig. 3.5). 2D-seismic data can only be migrated along the seismic line, decreasing the Fresnel zone to an ellipsoid perpendicular to the seismic line. In 3D-seismic, the data could be migrated both along and in perpendicular directions resulting in a Fresnel zone shaped as a circle with a small radius (Brown, 1999).

$$Hr = \frac{\lambda}{4} \tag{3.6}$$

Equation 3.6: Hr = Horizontal resolution (m), λ = Wavelength (m).

The horizontal resolution is calculated at approximately 25 m.

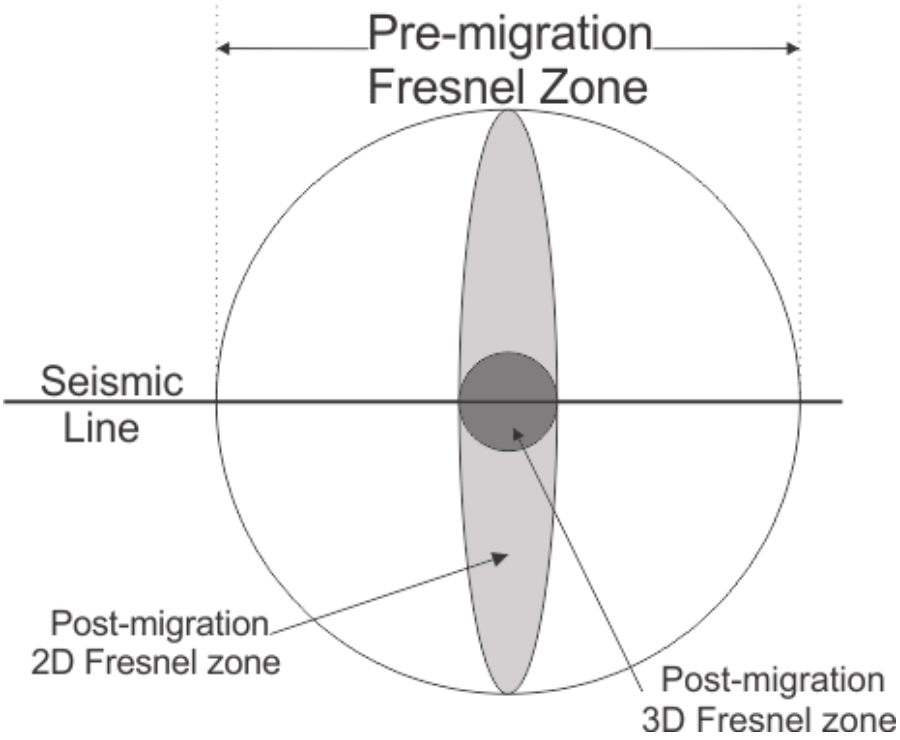

Figure 3.5: An illustrations of the Fresnel zone difference using pre- and post- migrated data. Using migration in 2D-data, the Fresnel zone shrinks largely along the seismic line forming an ellipsoid. On 3D-data another seismic line is shot perpendicular to the first, with migration shrinking the zone in this direction as well, ultimately creating a zone formed as a small circle. Figure modified from Brown (1999).

3.4 Artefacts

The seismic survey do to some degree contain artefacts in form of survey footprints (Fig. 3.6). Survey footprints are systematic noise that correlate with the acquisition geometry, and can be spotted in the seismic as linear lines parallel to the inline sampling direction (Bulat, 2005). It is important to be aware of artifacts in seismic as it complicate the interpretation process, and to identify them in order not to be mistaken as real features.

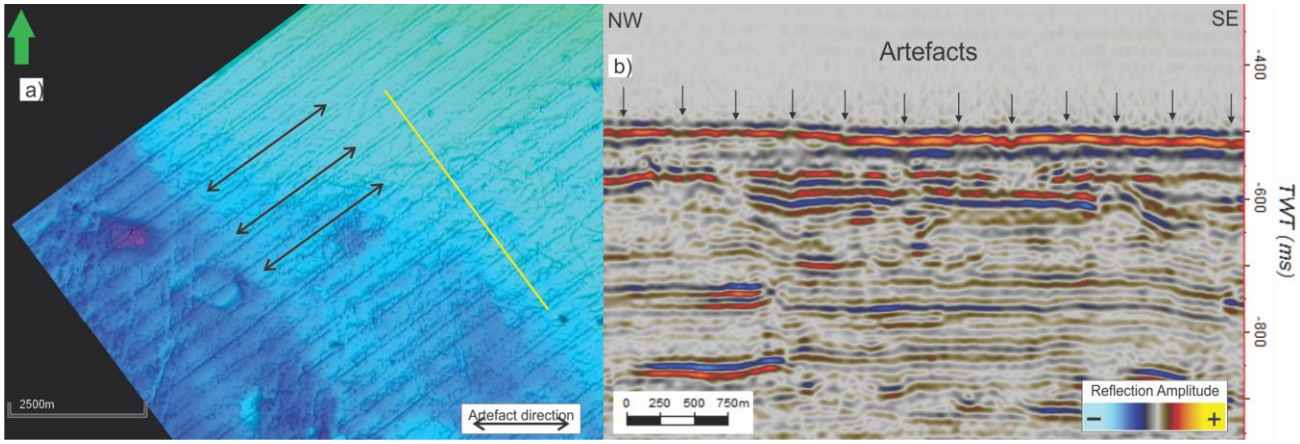

Figure 3.6: a) Display of the seafloor in the dataset with artefacts (survey footprints) parallel to the seismic inlines. b) Seismic intersection in crossline direction shown as the yellow line in a).

3.5 Interpretation method

The dataset used in this study is visualized and interpreted using the Petrel 2014 software from Schlumberger. The Petrel Software contain a number of tools and features that have been used for seismic analysis, interpreting paleosurfaces and generating seismic attributes from surfaces and volumes. The figures published in the study have been made and modified using CorelDRAW X6 software from Corel Corporation.

3.5.1 Interpretation of the seismic data

This study focus on the Snadd Formation, making deeper parts of the dataset little to non-interesting. Therefore, the dataset was cropped, deleting all seismic data with a two-way travel time higher than 3500 ms. The seismic horizons of this study were interpreted using seeded 2D- autotracking, interpreting every 10-100 inline and/or crossline and/or arbitrary line (perpendicular to fault systems). For "filling" the spaces between the interpreted lines this study used the Paintbrush and 3D autotracking functions.

3.5.2 Seismic attributes and well logs

The RMS Amplitude attribute highlights strong amplitudes within a targeted volume. The seismic attribute calculate the square root of the sum of squared amplitudes divided by the number of samples (Schlumberger, 2010). The attribute was used to interpret the different depositional environments and their depositional features.

The Isochron time-thickness attribute calculates the two-way travel time thickness between two seismic surfaces. Used to describe the thickness and extent of each of the seismic units.

The Gamma ray log measures the naturally occurring gamma rays in the formations adjacent to the wellbore, indicating the amount of radioactive content in the formations. The log is important in order to distinguish discrete differences in the sediment composition. As the log often responds different to shaly, silty and sandy deposits (shale has high values, sand has low), it is an important tool interpreting the depositional processes and environment.

4. Results

4.1 The Snadd Formation

The extent and volume of the Snadd Formation have been interpreted using well tops (NPD, 2016) from well 7222/11-1 as guidelines, mapping their corresponding reflectors. The Snadd Formation contain a number of consistent, high amplitude seismic markers, or possible flooding surfaces, which can be correlated seismically for hundreds of kilometers. These seismic markers or reflectors delimit the formation into seismic sub-units, possibly related to changes in the depositional environment (e.g. Glørstad-Clark et al., 2010). This study map and interpret a total of six reflectors, including the Top Kobbe and Top Snadd reflectors, which divides the Snadd Formation into five seismic units (Fig. 4.1).

The formation is at its thickest in the western part of the study area, with a measured thickness around 1000 ms (twt). The formation further thins eastward with thicknesses reaching 350 ms (twt) in the easternmost parts (Fig. 4.2).

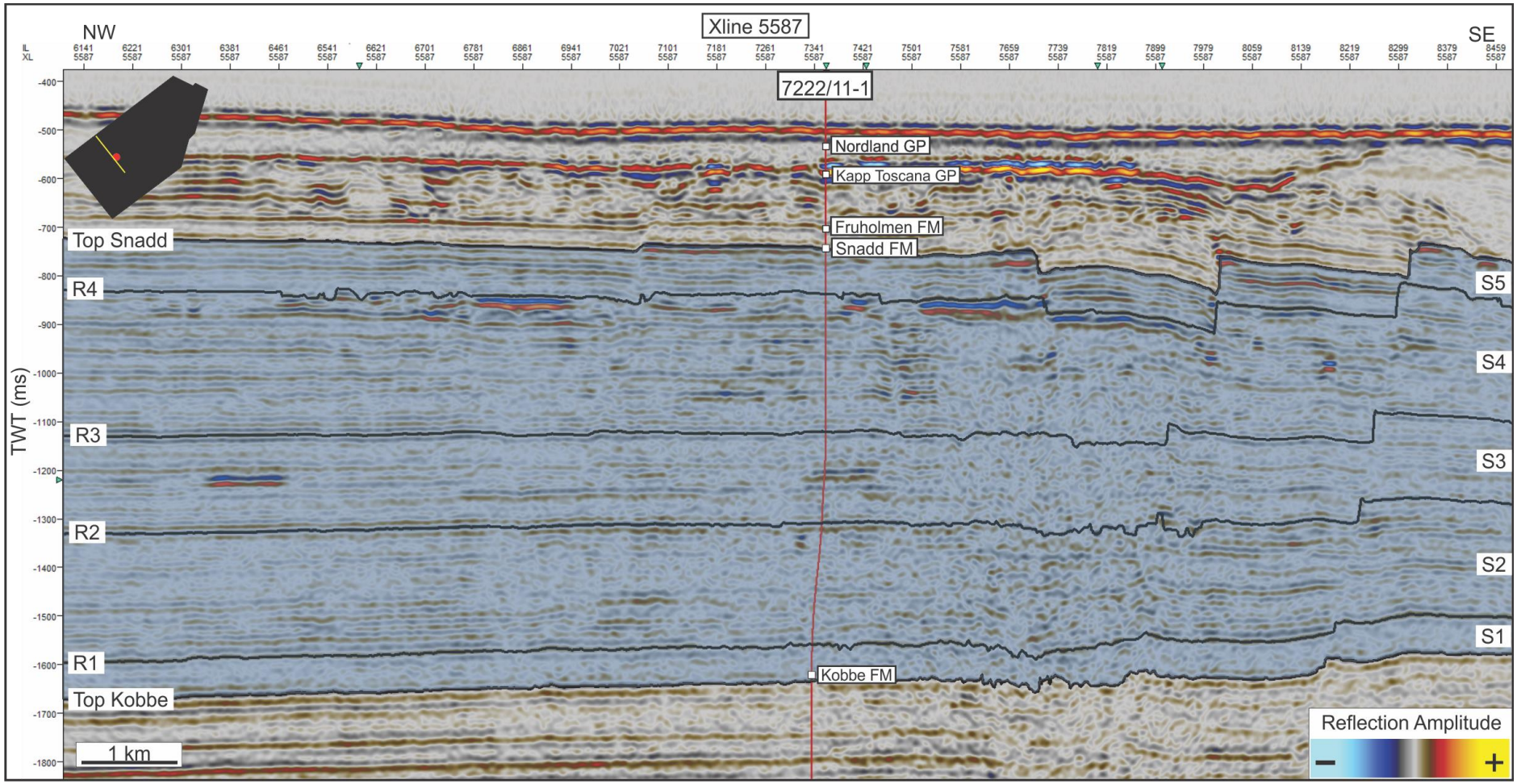

Figure 4.1: Seismic section illustrating the Snadd Formation in blue with the interpreted reflectors and units of the study. The black lines illustrates the six interpreted reflectors, separating S1-S5. The red line show the well 7222/11-1 and its interpreted well tops. Well tops from NPD (2016).

The post-Snadd stratigraphy have been eroded by deep canyons cutting into the upper part of the Snadd Formation, affecting the two uppermost interpreted reflectors (Top Snadd and Reflector 4) in the study area (Fig. 4.2).

The seismic signal has been highly affected by faulting, especially in the transition zone between the Loppa High and the Hammerfest Basin, making interpretation and mapping of the reflectors difficult in this area. The fault zone is indicated in Figure 4.2A.

The survey also include two sets of small scale fault systems, located in the southern and eastern parts. The southern fault system has a W-E orientation trend, while the eastern system has an orientation trend going NE-SW, somewhat corresponding to the large scale fault zone (Fig. 4.2A).

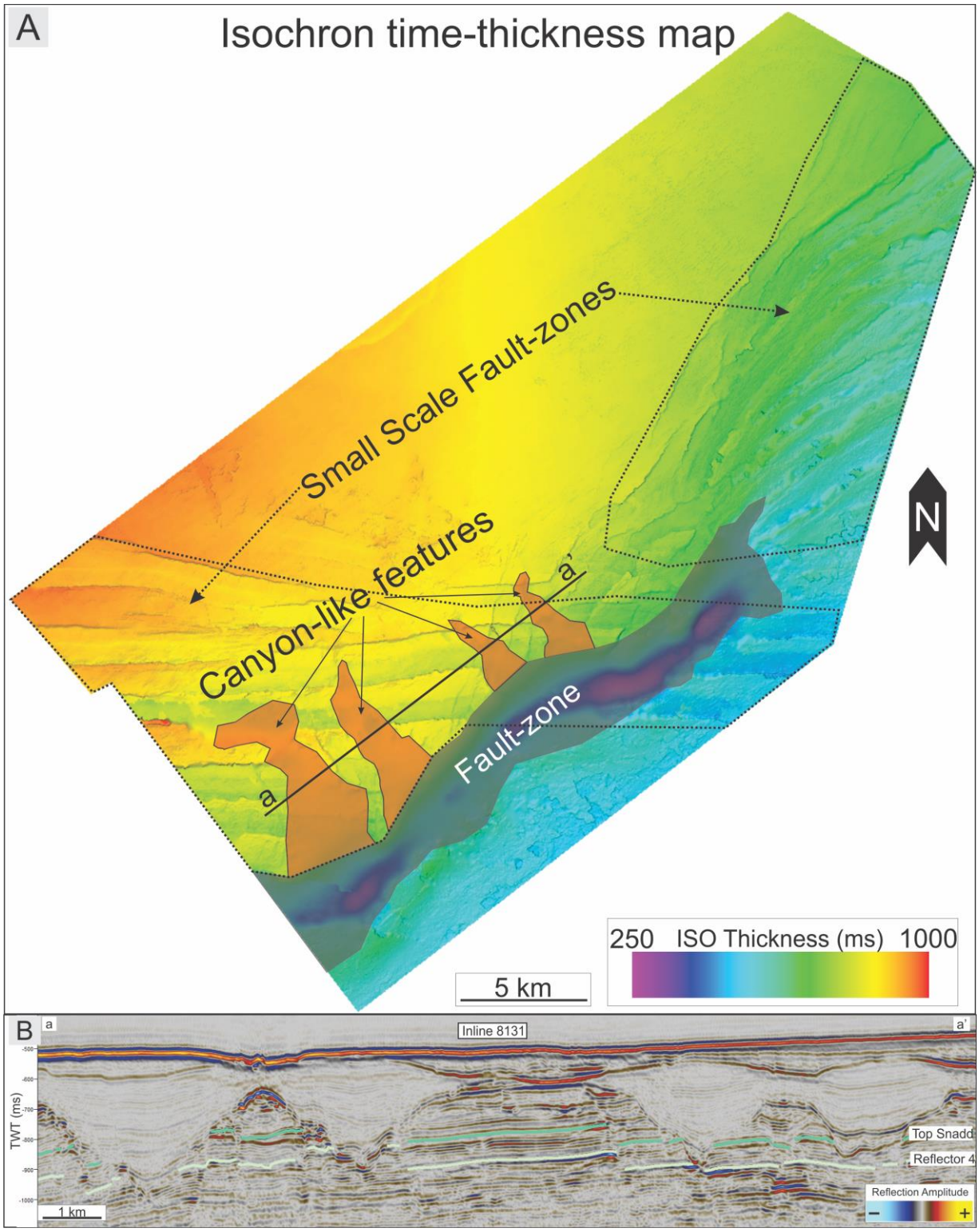

*Figure 4.2: **A**: Isochron time-thickness map showing the two-way travel time millisecond thickness variation of the Snadd Formation in the data set. Features interfering with the formation are also highlighted. **B**: Seismic section illustrating the correlation between the canyon-like features and the seismic reflectors. Location of the line is shown in A.*

4.2 Intra Snadd reflectors

The formation is limited and divided by a total of six reflectors, including the Top Kobbe and Top Snadd reflectors, delimiting the formation into five sub-units.

The Top Kobbe reflector represent the boundary between the overlying Snadd Formation and the underlying Kobbe Formation, and the base of a series of concordant to gently inclined reflections. The negative seismic reflection has a relatively high continuity with a medium to high amplitude throughout the whole study area. The reflector has a southeastern dipping trend, with depths ranging from -1520 to -2560 ms (twt) (Fig. 4.3F).

Reflector 1 (R1), which represents the top of seismic **sub-unit S1** and the lowermost interpreted internal reflector in the Snadd Formation, is gently downlapped or baselapped by the overlying unit and characterized by concordance. R1 is somewhat parallel to the 50- 70 ms (twt) underlying Top Kobbe reflector and can further be described as a highly continuous reflector with a medium positive amplitude (Fig. 4.3E).

Reflector 2 (R2) represents the top of seismic **sub-unit S2,** and is located about 200 ms above Reflector 1, with depths ranging from -1250 to -2300 ms (twt) dipping southeastwards (Fig. 4.3D). The reflector can be described as mostly continous with a medium negative amplitude, and can be characterized by concordance.

Reflector 3 (R3) represent the the top of the seismic **sub-unit S3** with depths ranging between -1050 to -2200 ms (twt) (approximately 100- 200 ms above Reflector 2), with a southeastern down dipping trend (Fig. 4.3C). The reflector has a medium positive amplitude and can be described as continous to discontinuous, gently toplapped by the unit below and characterized by concordance.

Reflector 4 (R4) represent the top of the seismic **sub-unit S4** with depths between -800 to -2050 ms (twt) (approximately 150- 250 ms above Reflector 3, 100 ms below the Top Snadd reflector), with a southeastern down dipping trend (Fig. 4.3B). Reflector 4 has a positive amplitude, and can be described as mostly continuous with low average amplitude values. The relationship with its surrounding reflectors is characterized by concordance.

The Top Snadd reflector represent the boundary between the underlying Snadd Formation and the overlying Fruholmen Formation with depths between -700 to -1950 ms (twt) (approximately 100 ms above Reflector 4), with a southeastern down dipping trend (Fig. 4.3A). The Top Snadd reflector is continuous, and has a large negative amplitude. The relationship with its surrounding reflectors is characterized by concordance.

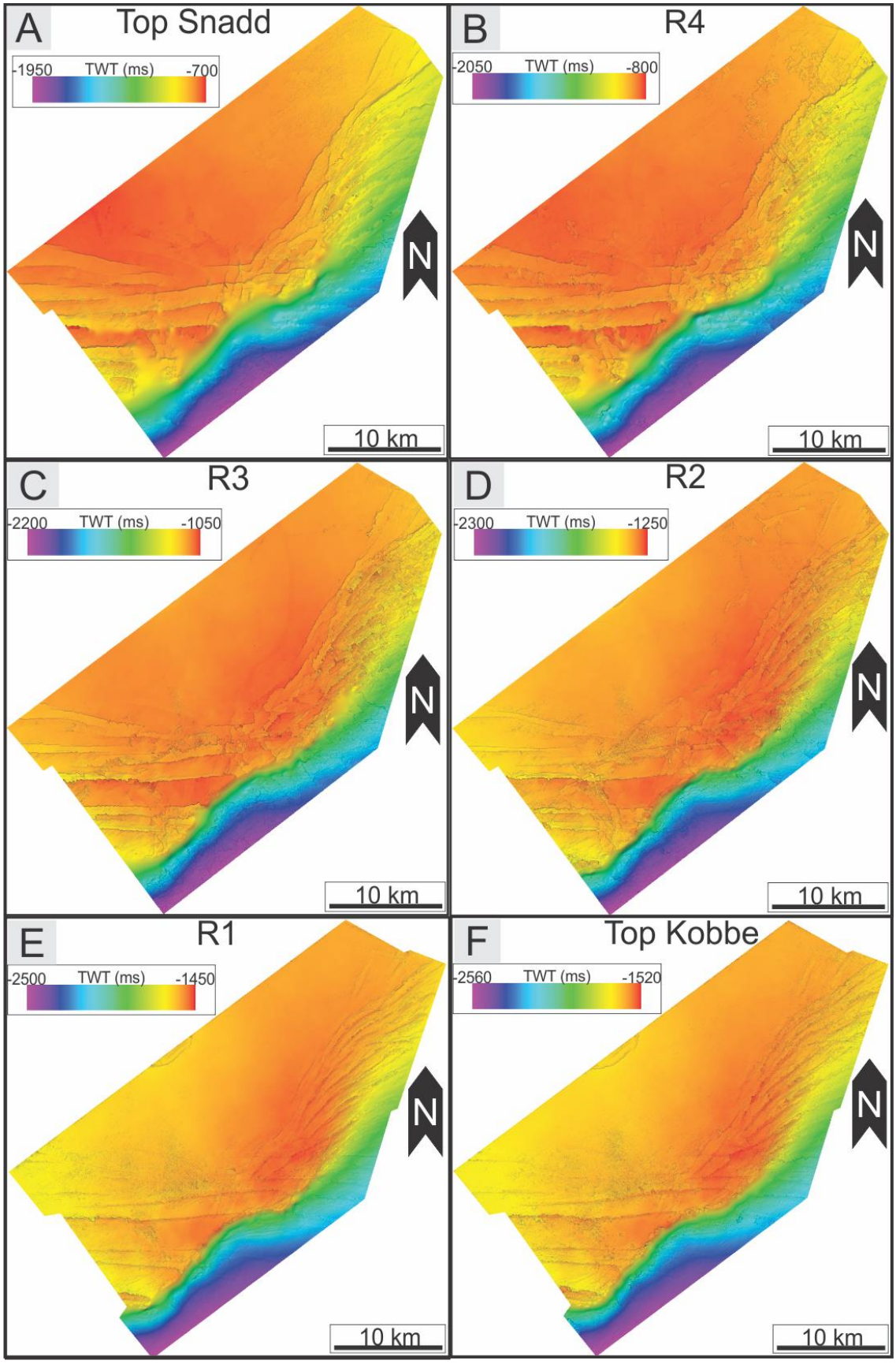

Figure 4.3: Time (twt) structure maps of the different internal reflectors interpreted within the Snadd Formation. Notice that the legend differs between the maps. ***A****: Top Snadd reflector.* ***B****: R4 reflector.* ***C****: R3 reflector.* ***D****: R2 reflector.* ***E****: R1 reflector.* ***F****: Top Kobbe reflector.*

4.3 Seismic units

By interpreting the six different reflectors, it is possible to divide the Snadd Formation into five seismic sub-units, where each reflector represents a transition to a new depositional environment. Figure 4.4 show the gamma ray log from exploration well 7222/11-1 drilled within the data set (Fig. 3.1). The most important thing to notice from the figure is the distinct change in gamma ray values at the interpreted R3 reflector.

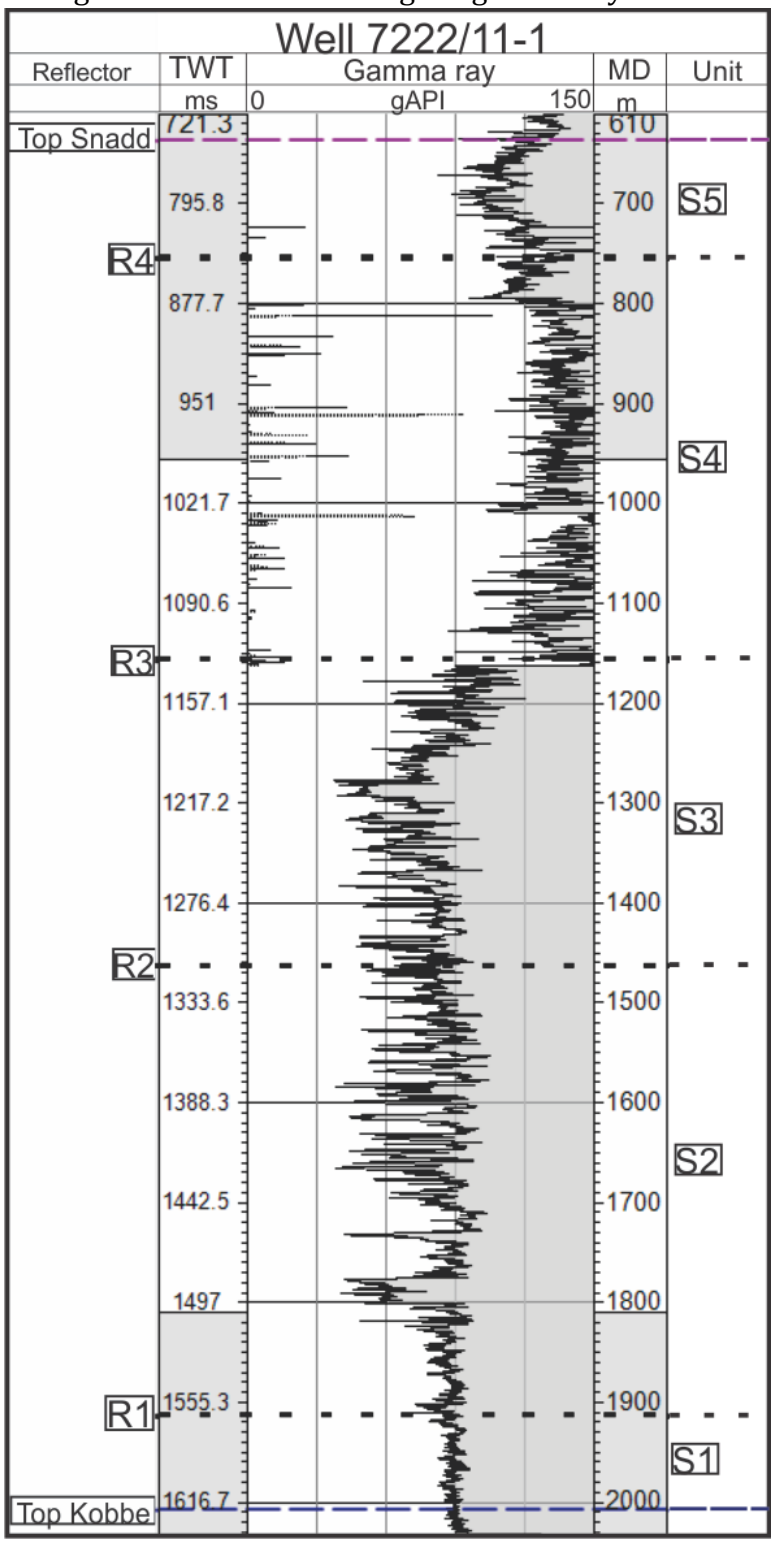

Figure 4.4: Well section of well 7222/11-1. From left to right: Margin indicate the different interpreted well tops and the additional four interpreted internal reflectors R1-R4. Column indicate the depth measured in TWT. Log showing the measured gamma ray within the Snadd Formation. Column indicating the depth measured in meters. Margin indicating the interpreted seismic units.

4.3.1 S1 - Unit 1

The lowermost unit interpreted in the formation is seismic unit S1, which is limited by the Top Kobbe- and R1 reflectors. The average TWT-thickness of the unit is approximately 60-80 ms (twt) (Fig. 4.5B). The unit represents a unit of low variation in the seismic signal with no clear features (Fig. 4.5C).

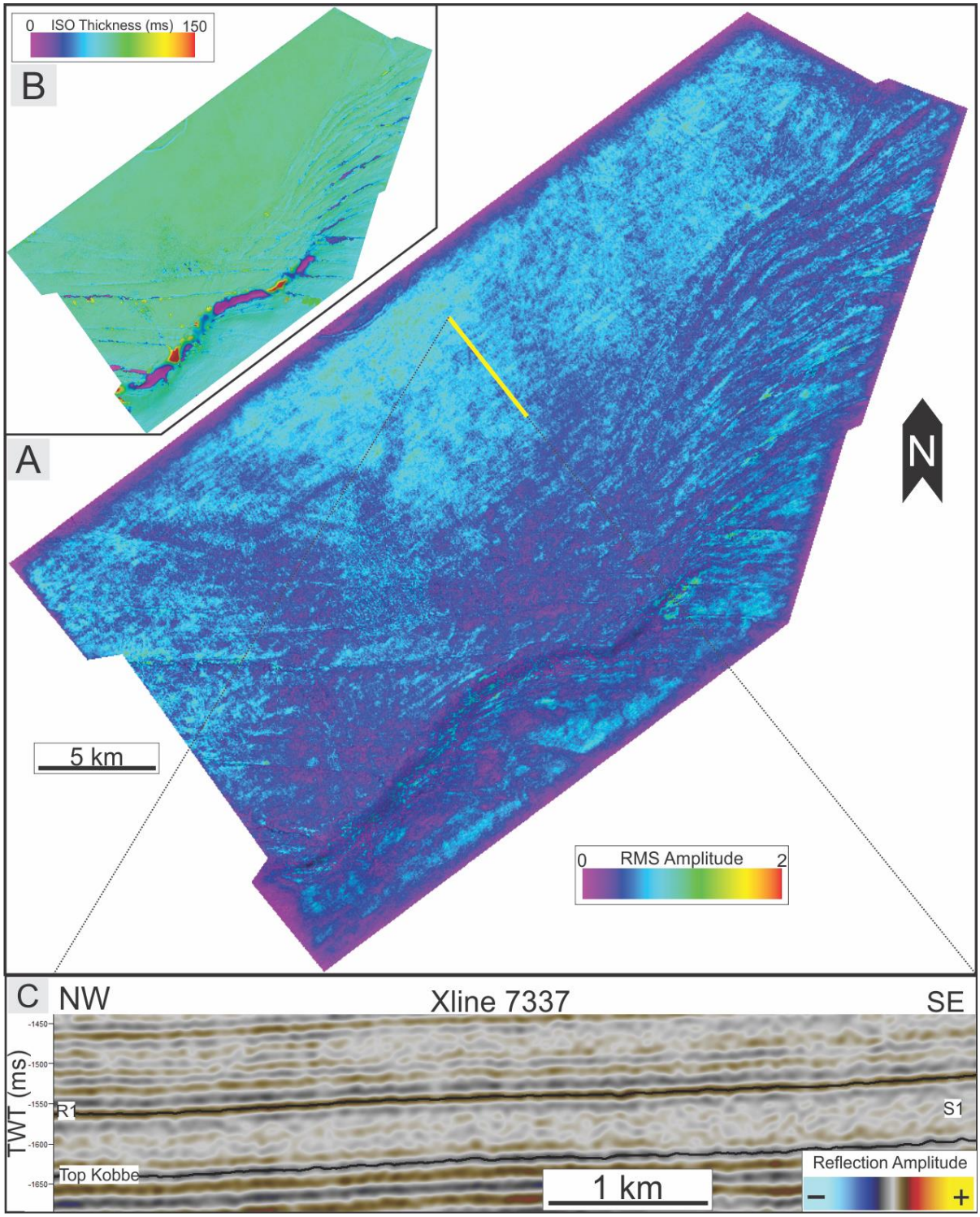

*Figure 4.5: **A**: RMS-map of seismic unit S1. The seismic section in C is highlighted. **B**: Isochron time thickness map of seismic unit S1. **C**: An example of a seismic section from Xline 7337 showing unit S1.*

The unit can be described as a thin, uniform seismic section. Reflection amplitudes within the unit are discontinuous and low, and can be characterized as transparent. The gamma ray log within S1 (Fig. 4.4) is stable, with medium values.

Interpretation: The S1 unit has no highlighting features. The unit has a uniform thickness of around 70 ms without any continuous reflector. The environment during deposition of S1 seems therefore to be very stable, without any influence from fluvial or alluvial processes. This is interpreted as a marine shelf environment.

4.3.2 S2 - Unit 2

The volume limited by the R1 and R2 reflectors is called the S2 unit. The unit is large with an average thickness of around 230 ms (twt) (Fig. 4.6B). The initial reflectors within S2 could be described as discontinuous with alternating amplitudes, containing a number of high-amplitude features, some of them extending for more than 5 km (Fig. 4.6A). It does not seem to be any regional orientation trend, and the features vary both in size and amplitude, with most being low-valued within in the RMS-map.

The seismic sections in Figure 4.6 show a number of small high-amplitude features within the S2 unit. Common for most of the features within S2 is that they are quite narrow (less than a kilometer wide) with the length varying between 2 km for the smallest ones and the largest up to about 10 km. All the small features seem to, at least to some extent, interfere with the reflectors below. It is important to notice that the different features observed in Figure 4.6 belongs to different stratigraphic levels within S2.

The large feature indicated in the lower part of the unit in Figure 4.7A is parallel to the surrounding reflectors, with an upper peak and a lower trough. This separates it from the other, smaller features observed further up in the section with clear upper troughs and lower peaks.

Figure 4.6C reveal a regional trend change, with the reflectors in the lower part of the unit being largely continuous with a somewhat high amplitude. The upper part of the unit on the other hand, has a much lower amplitude with a higher discontinuity. The same change can be seen in Figure 4.7B. The trend change occurs about 100 ms above the R1 reflector. By separating the S2 unit into two sub-units parted by the border 100 ms above the R1

reflector (Fig. 4.6C), this reveal clear differences between the upper and lower sub-units. Besides the large positive amplitude feature in the northern part of the data set, the lower sub-unit is almost completely uniform without any significant shapes or features (Fig. 4.8A). The feature is about 8 km long and 3 km wide, with a W-E direction.

The RMS map of the upper sub-unit (Fig. 4.8B) differs from the lower one, with a generally lower amplitude, but with a higher density of high-amplitude features. In general, the features seem to have an upper trough and a peak base, with examples shown in Figure 4.7. In the northern half of the data set, it could be a possible NW-SE directional trend on many features. The trend is though not obvious. Except for a couple of large features longer than 10 km, the sizes seems to be smaller than 8x1 km.

The gamma ray log indicate (Fig. 4.4) that the S2 unit could be divided into two halves. The lower sub-unit (up to about 1700 MD) show stable medium values, with two incidents with significant lower measurements. Above 1700 MD the log has an average medium value, but with much larger variations than the lower sub-unit.

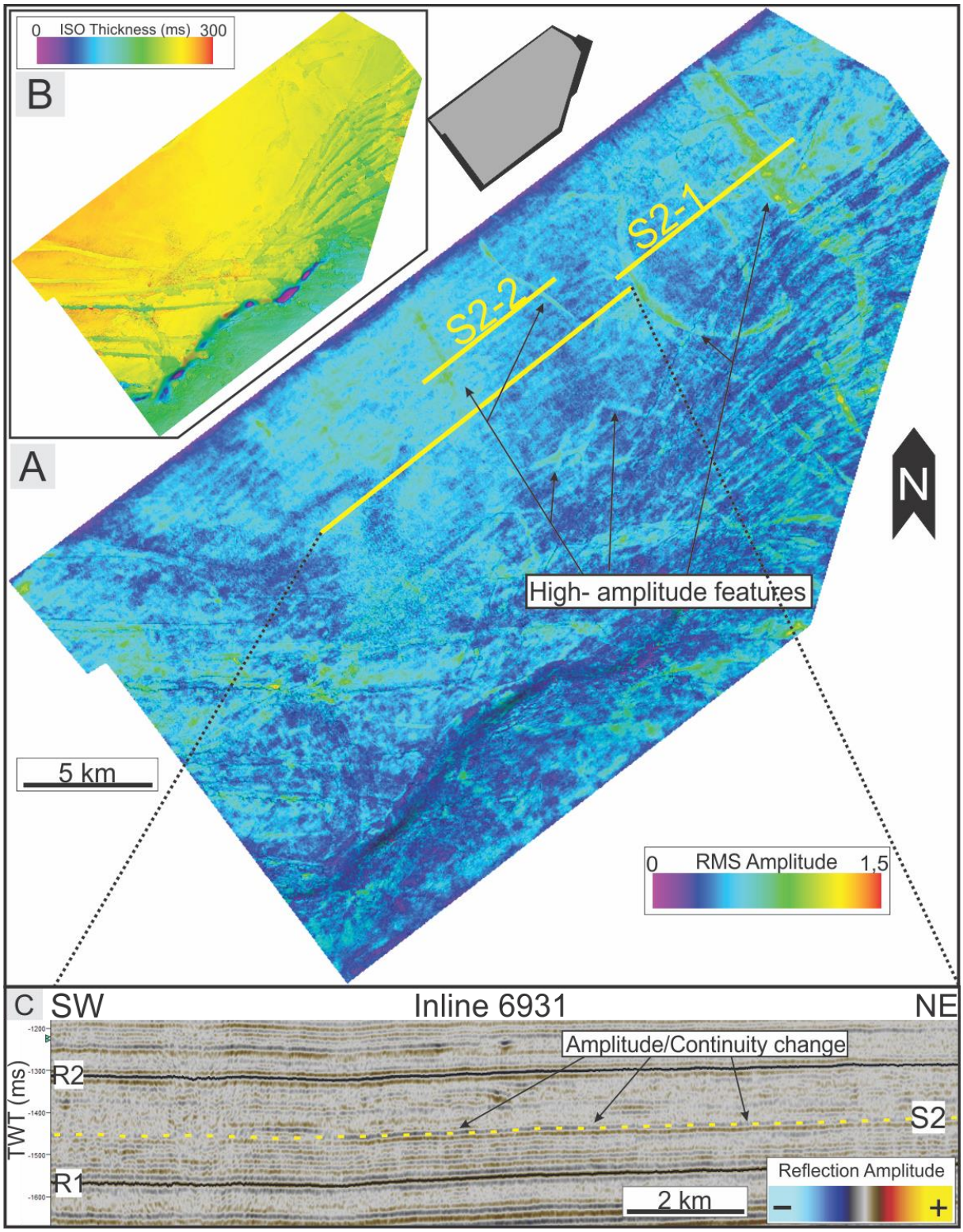

*Figure 4.6: **A**: RMS-map of seismic unit S2. The seismic sections from Figure 4.7 are highlighted in yellow. **B**: Isochron time thickness map of seismic unit S2. **C**: Seismic section at Inline 6931 highlighting some characteristics within the S2 unit. The yellow dotted line splits the unit into two sub-volumes used in Figure 4.8.*

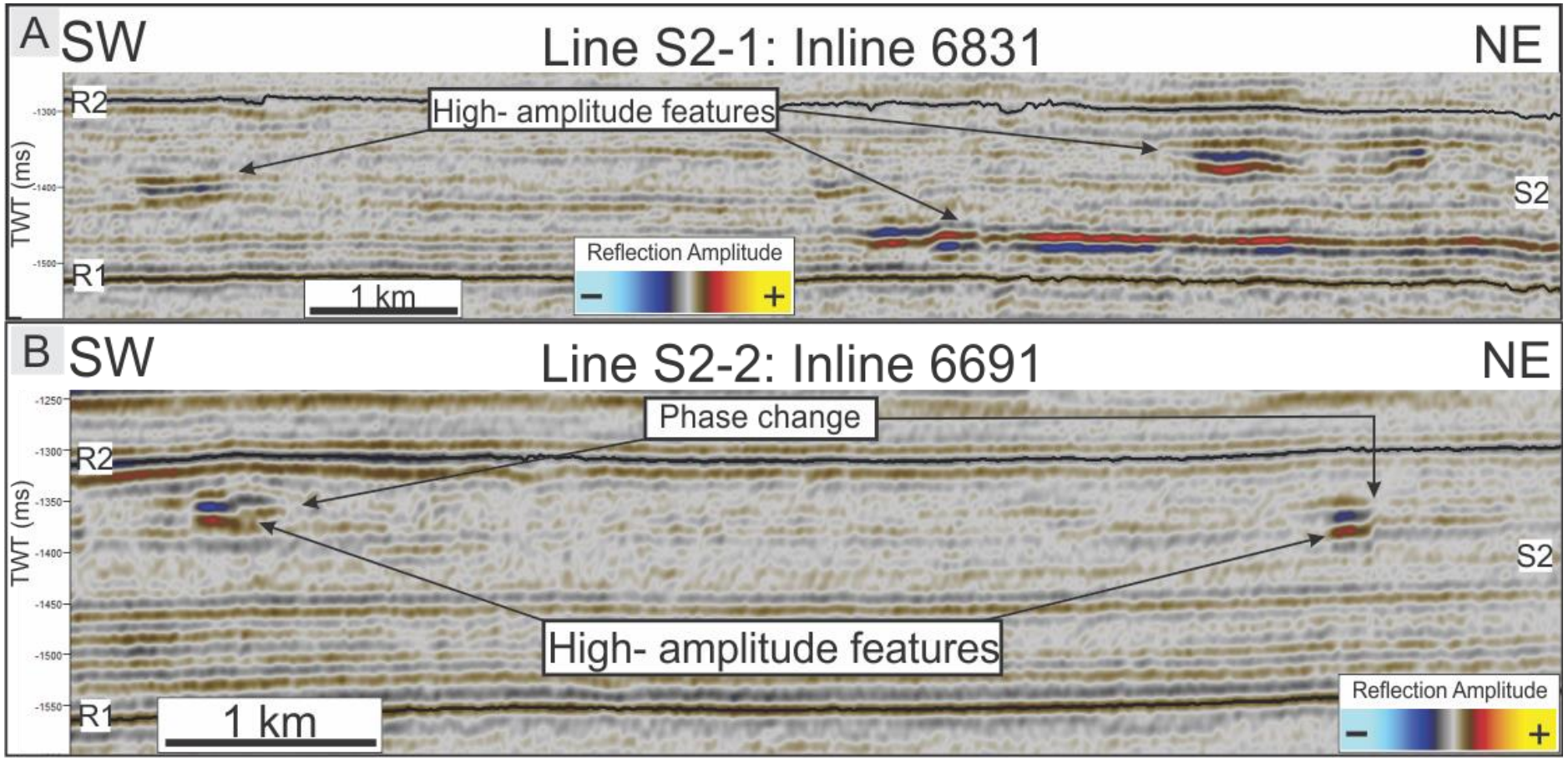

*Figure 4.7: Two different seismic sections showing high-amplitude features at the S2 unit. **A**: Seismic section from Inline 6831 showing three different features of high amplitude. **B**: Seismic section from Inline 6691 showing two features of high amplitude*

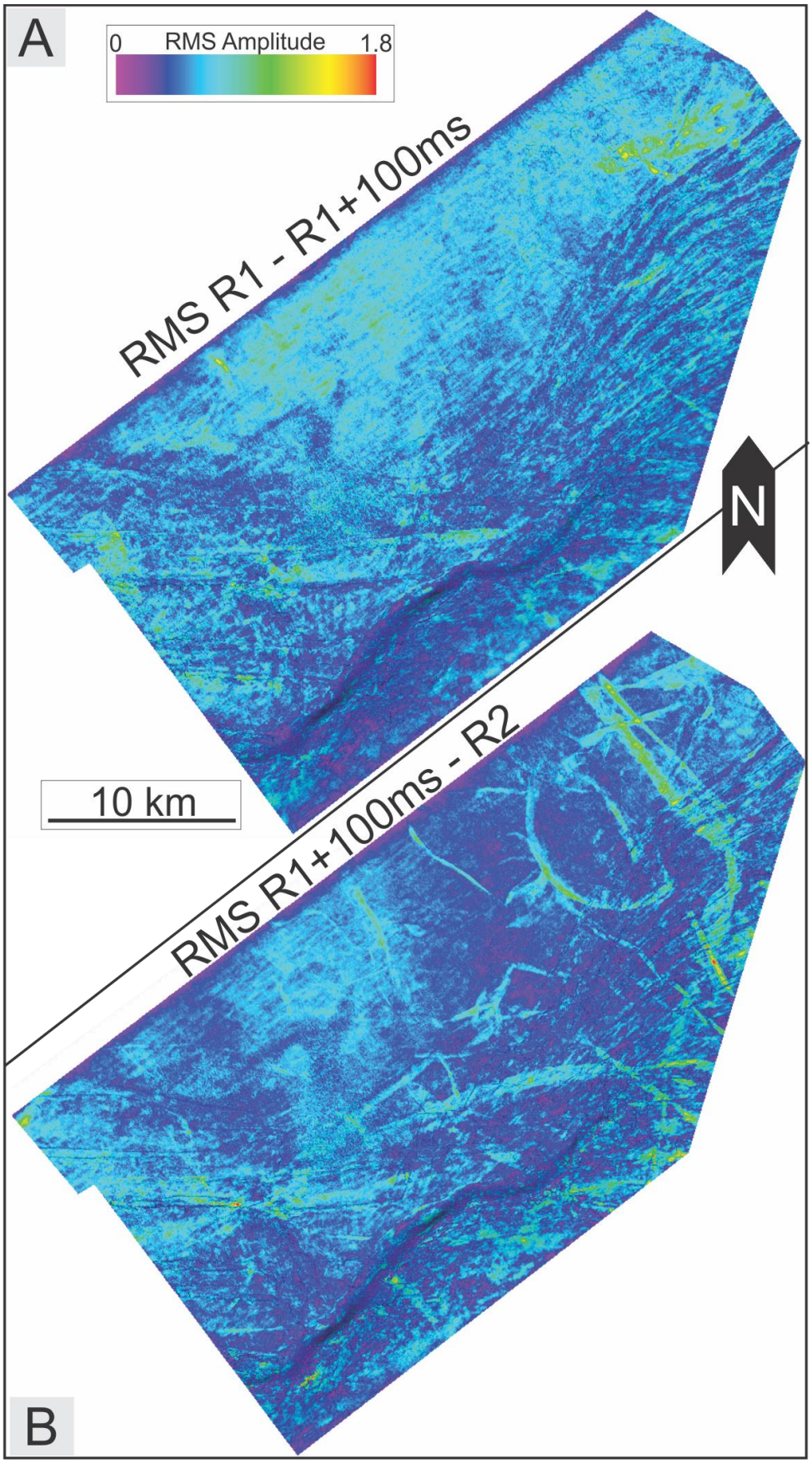

Figure 4.8: The S2 unit divided into two sub-units. Volume illustrated in Figure 4.6C. ***A****: RMS-map extracted from the volume between the R1 reflector and 100 ms above the R1 reflector (yellow dotted line).* ***B****: RMS-map extracted from the volume between 100 ms above the R1 reflector (yellow dotted line) and the above lying R2 reflector.*

Interpretation: There is clearly a change in the depositional environment within unit S2 (Fig. 4.6C). This assumption is confirmed by the two RMS-maps shown in Figure 4.8 together with the gamma ray log in Figure 4.4.

The lower sub-unit is characterized by continuous, high-amplitude, concordant reflectors and stable gamma ray values, which is interpreted to represent a shallow marine environment. The two gamma ray cases with lower values suggests episodes of sand in an overall shaly environment. This combined with the possibly correlating feature found about 50 ms above R1 (Fig. 4.8A), makes a short change from a marine shelf to a coastal setting likely.

The upper sub-unit characterization with discontinuous, low- amplitude reflectors combined with a more unstable gamma ray log suggests a change in the dominant depositional regime to a coastal plain environment. The environment is largely influenced by low-acoustic features with variating sizes, interpreted to be of fluvial origin.

4.3.3 S3 - Unit 3

Unit S3 covers the middle part of the formation limited to the volume between the R2 and R3 reflector, at an approximate average thickness of 170 ms (twt). S3 contain an area of large, straight, close to parallel, high-amplitude features with upper troughs and lower peaks. The RMS-map also reveal about four to five smaller features, crescent shaped, with a size between one and three kilometers in maximum length. The features can be characterized by the half-circular shape and the multiple, small, sub-parallel reflectors.

The largest linear feature is 1 km wide and at least 12 km long, and seems to continue out of the data set (Fig. 4.9A). Moving 1 km east, another feature with about half the size of the large one (500 m wide, ca 8 km long) show a possible trend with an SSW-NNE direction. The area has an overall higher amplitude than the surroundings, and also show some smaller features with the same trend. The overall high amplitude trend in the western area seem to come from a different reflector about 50 ms below the reflector with the largest, high amplitude feature (Fig. 4.10A, B).

In order to investigate the features in further detail, Figure 4.11 separates the two seismic events into two different, RMS maps, with A being generated between 25-75 ms above R2, while B between 75-125 ms above R2. The maps clearly reveal that the smaller parallel features, together with the smaller crescent shaped features, have been created during the same timeperiod in an otherwise uniform depositional environment (Fig. 4.11A). Figure 4.11B reveal that besides the feature similar to the ones found in Figure 4.11A, the section could be described as conformable with low seismic variations. However, the feature found are even larger and with a higher amplitude than the ones below. All of the features in the S3 unit has an upper trough and a lower peak.

Seismic sections of the different features are visualized in Figure 4.10, with A and B showing the large features within the unit. Figure 4.10C show a cross section at one of the smaller features. Here it is important to notice how the amplitude value changes within the features.

The gamma ray log within S3 (Fig. 4.4) can be divided due to its characteristics. The lower part (below 1300 MD) have medium values with large variations. Above, there is an around 25 meter thick event of lower, more constant values. The top sub-unit show

increasing values and variations, from a constant, medium at 1275 MD, to medium-high just below R3 (1160 MD). At R3, there is a sudden log increase, with high GR-values.

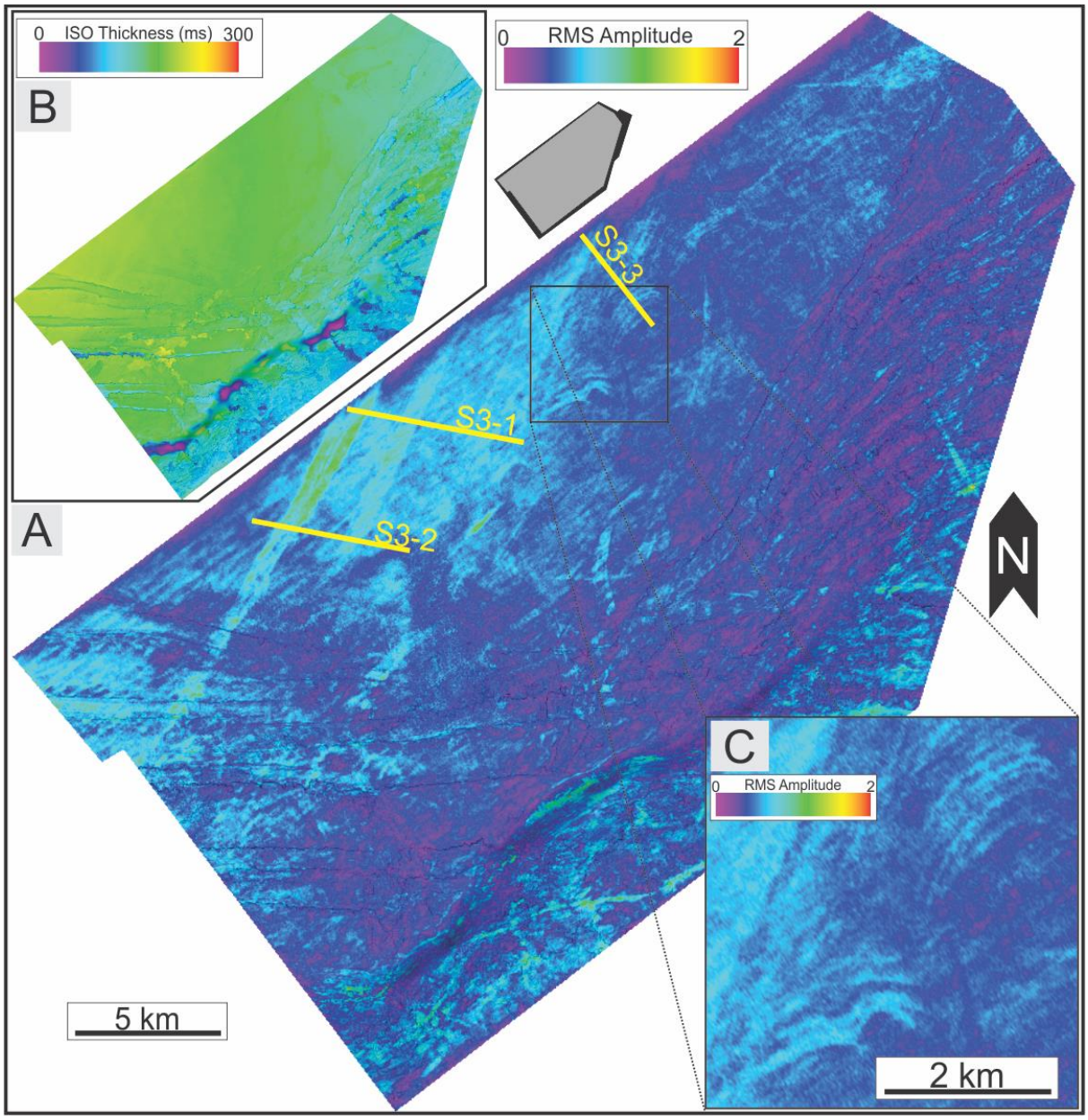

*Figure 4.9: **A**: RMS-map of seismic unit S3 with the seismic sections from 4.10 highlighted. **B**: Isochron time thickness map of seismic unit S3. **C**: Zoom-in figure of small, crescent shaped features.*

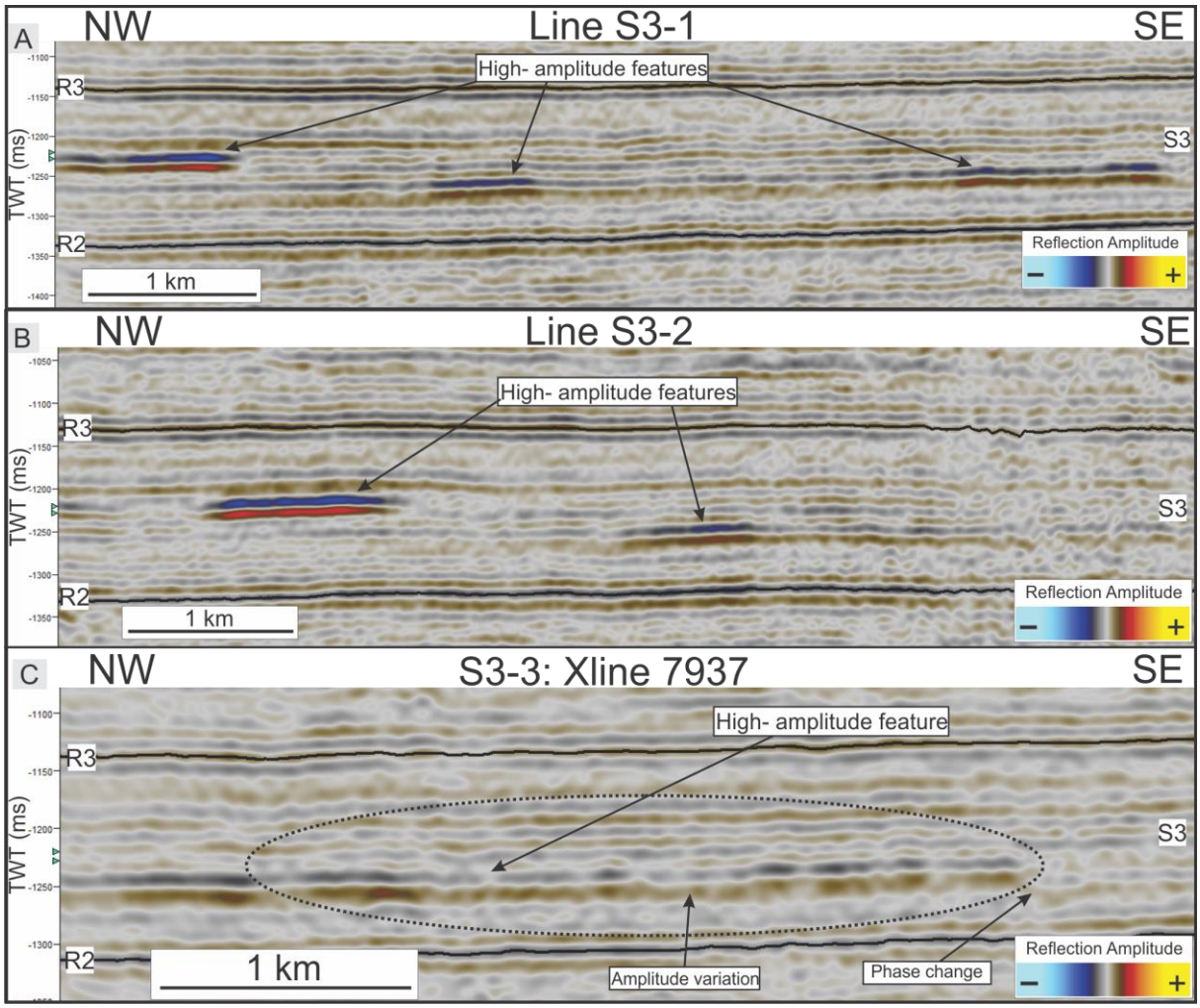

Figure 4.10: Three seismic sections showing the different high-amplitude features within the S3 unit. Locations of the lines are shown in Figure 4.9. ***A****: Seismic section from the arbitrary line S3-1 perpendicular to the large parallel features.* ***B****: Seismic section from the arbitrary line S3-2 perpendicular on the large parallel features.* ***C****: Seismic cross section at Xline 7937 of the smaller, crescent shaped features marked as high amplitude feature.*

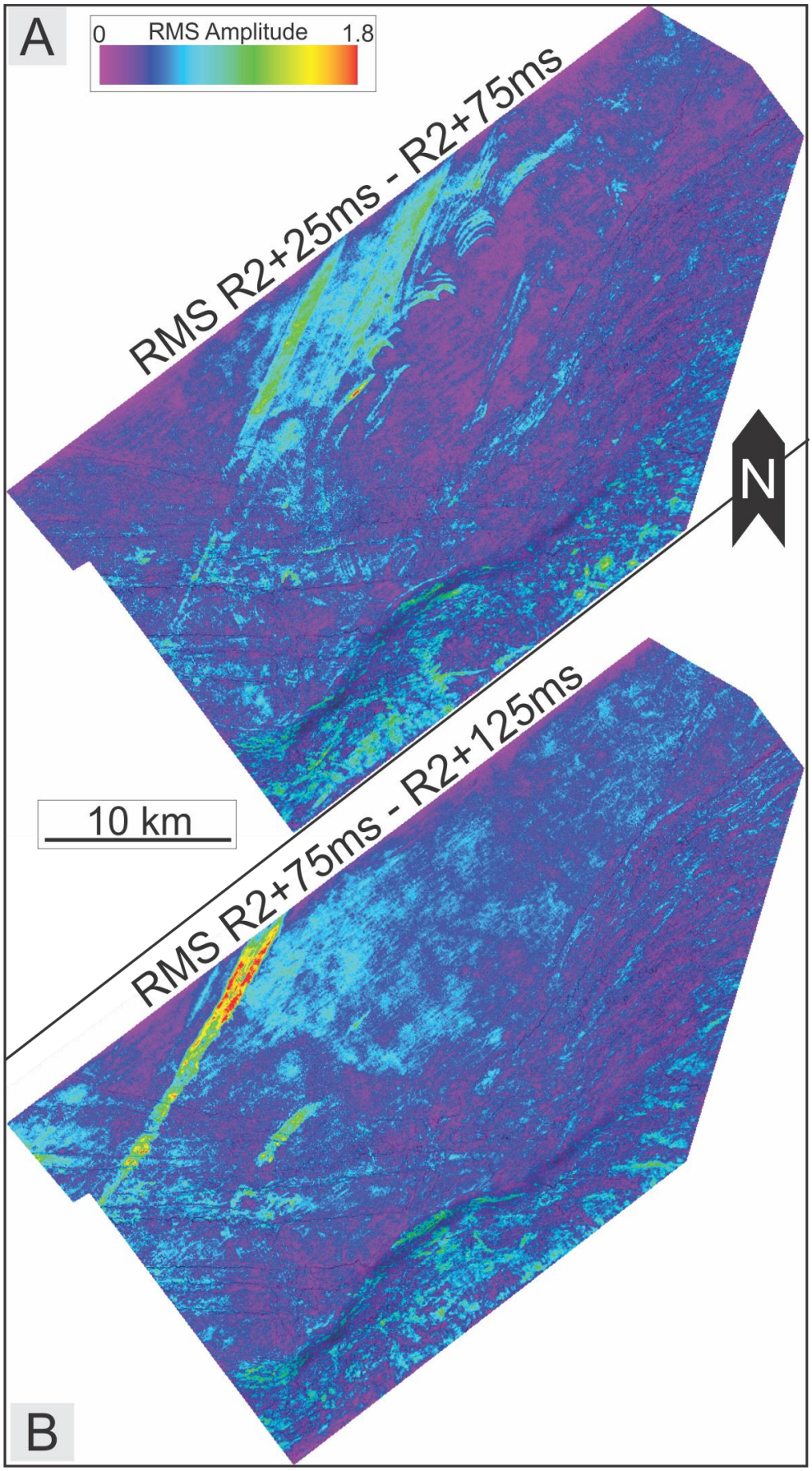

Figure 4.11: RMS-maps of two sub-units within the S3 unit. ***A****: RMS-map extracted from the volume between 25 ms above the R2 reflector and 75 ms above the R2 reflector.* ***B****: A RMS-map extracted from the volume between 75 ms above the R2 reflector and 125 ms above the R2 reflector.*

Interpretation: The small half-circular shaped features within the lower part of S3 (Fig. 4.9C) are likely aeolian barchan dunes. These shapes are widely recognized in aeolian depositional environments. The lower part of S3 also have a large high amplitude feature extending through large parts of the data set. Similar features are also found further up in the stratigraphy. The seismic sections crossing these, show no signs of an erosive base or infill, but the features has a lower acoustic impedance than the surroundings. This, together with the perfectly straight shape in horizontal direction, suggests that the features are of non-fluvial origin. The low measured values within the log suggest a sandy environment. These could then be interpreted as beach ridges or barrier islands.

4.3.4 S4 - Unit 4

Limited by the R3 and R4 reflectors, S4 is the thickest unit with an approximate 250 ms (twt) average thickness (Fig. 4.12B). Figure 4.12 show one large feature, which is more than 20 km long and 1 km wide, extending from the northern to the southwestern part of the survey. The southwestern part of the study area has also a couple of smaller features, possibly connected to the large structure.

Further examination reveal the presence of other, smaller features in lower parts of the unit. The observed features are in general of lower acoustic impedance with an upper trough and a lower peak. The RMS map in Figure 4.13 is generated from a lower part of the unit, within a volume between 50-100 ms above R3. The sub-unit includes a series of smaller, subparallel features in central parts of the study area with a NW-SE orientation. The features are about 10 km long and individually less than a kilometer wide, and are spread over a distance of 5 km. The map also show a possible outline of a larger NE-SW orientated structure in the same area.

The main feature in S4 is located within the top 50 ms (twt) of the unit (Fig. 4.14). It is about 25 km long and 1-1,5 km wide, ranging from the top northern corner of the data set to the south-central part with two smaller curves in the northern half, and a larger curve near the southern end. Figure 4.14 show a clear amplitude rise in the feature, halfway between line R4-1 and R4-2. North of this change the RMS-amplitude is generally much lower than in the southern part. Further examination of the feature in Figure 4.15A & B reveal a clear discontinuity in the reflectors, with the feature having an upper trough, a

lower peak and a possible prograded fill. In some areas the distance between the top relief and the bottom of the structure is more than 50 ms (twt). Figure 4.15C maps the regional extent and change, showing how the feature develops within the study area.

The RMS-map over R4 also highlights a couple of side features seemingly connected to the main one. These features have the same high amplitude as the main feature, but is shorter (no longer than 10 km) and widths seldom exceeds 1 km.

The gamma ray log in S4 (Fig. 4.4) show generally high values with medium to high variations. The log reveal three upwards increasing GR sequences. The upper part of S4 include an event of a bit lower GR values. The well discovered hydrocarbons in the upper part of the unit (NPD, 2016).

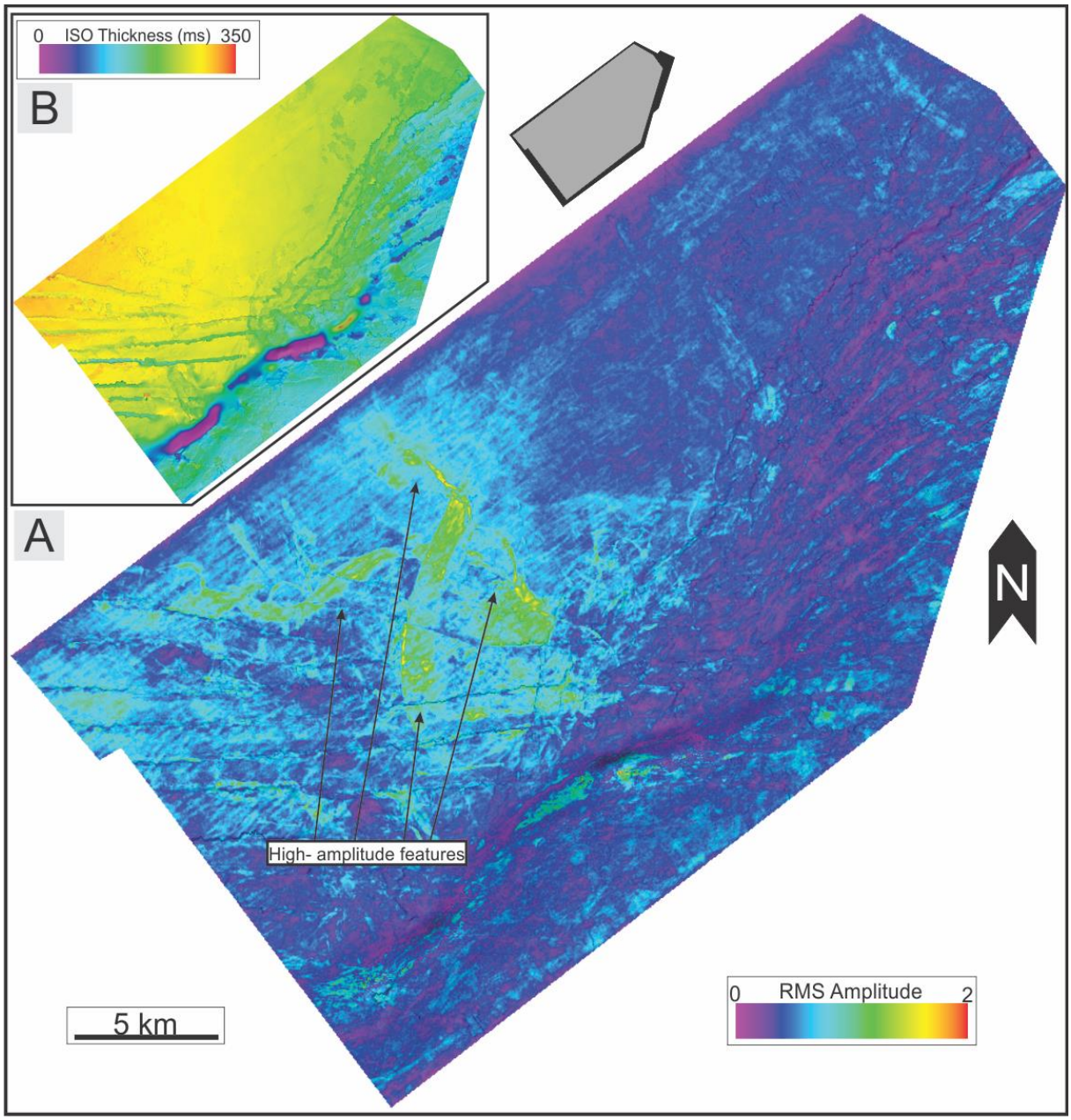

*Figure 4.12: **A**: RMS-map of the total seismic unit S4. **B**: Isochron time thickness map of the seismic unit S4.*

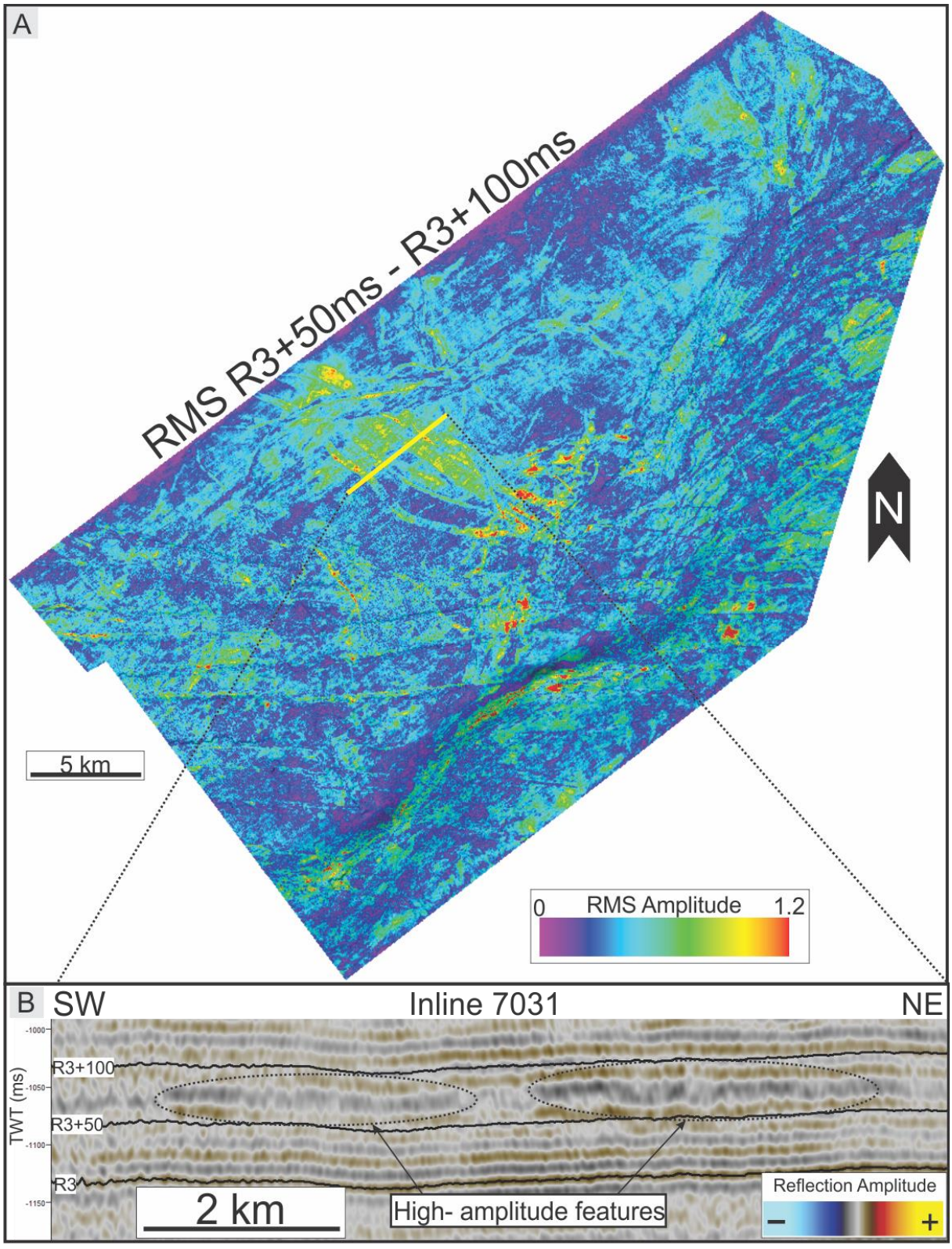

*Figure 4.13: **A**: A RMS-map extracted over the volume between 50 ms above the R3 reflector and 100 ms above the R3 reflector. **B**: Seismic section at Inline 7031 identifying some of the high amplitude features shown in A.*

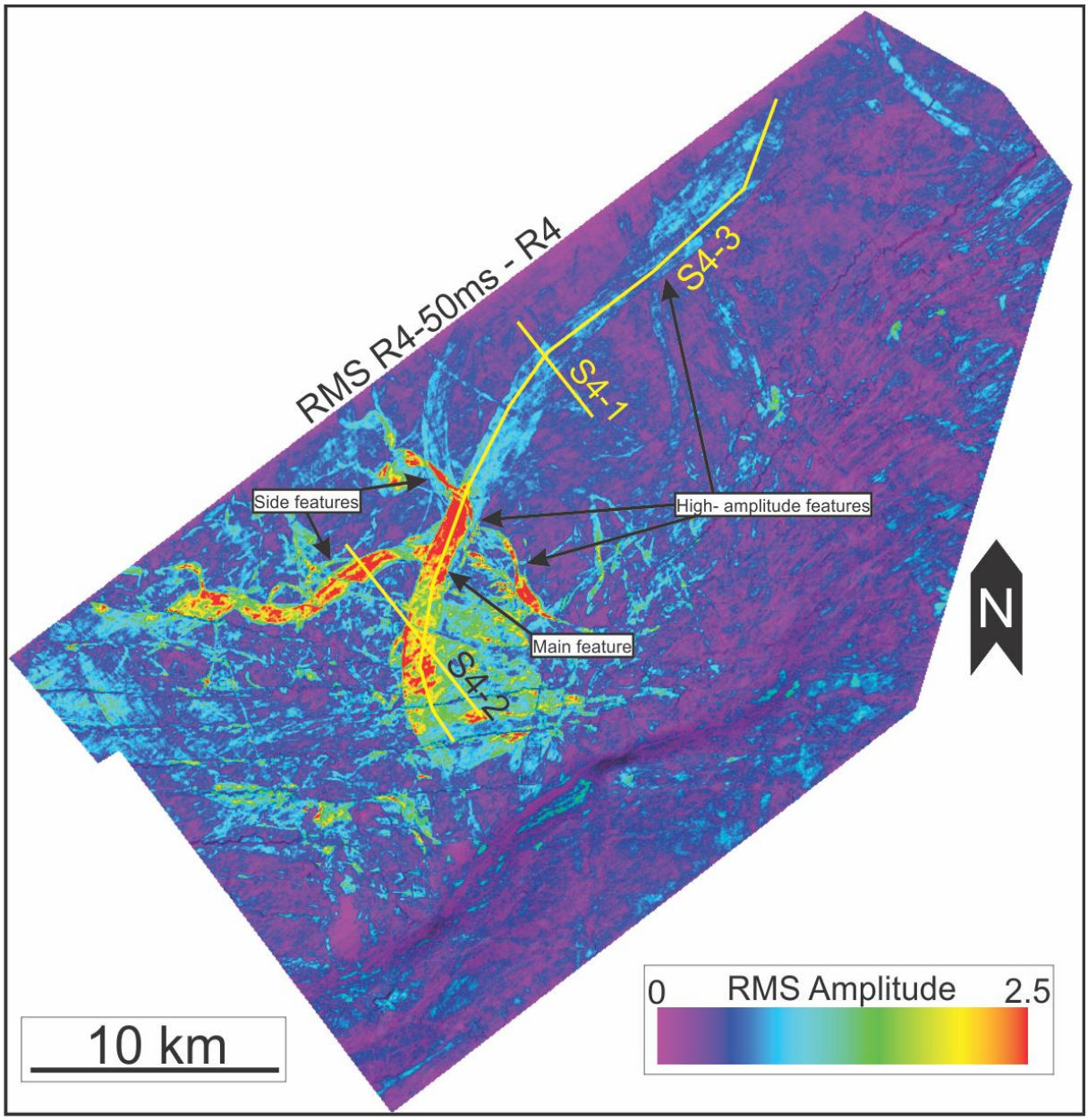

Figure 4.14: RMS map extracting the high amplitude features found in the volume between 50 ms below the R4 reflector and the R4 reflector. Yellow lines represent the seismic sections in Figure 4.15.

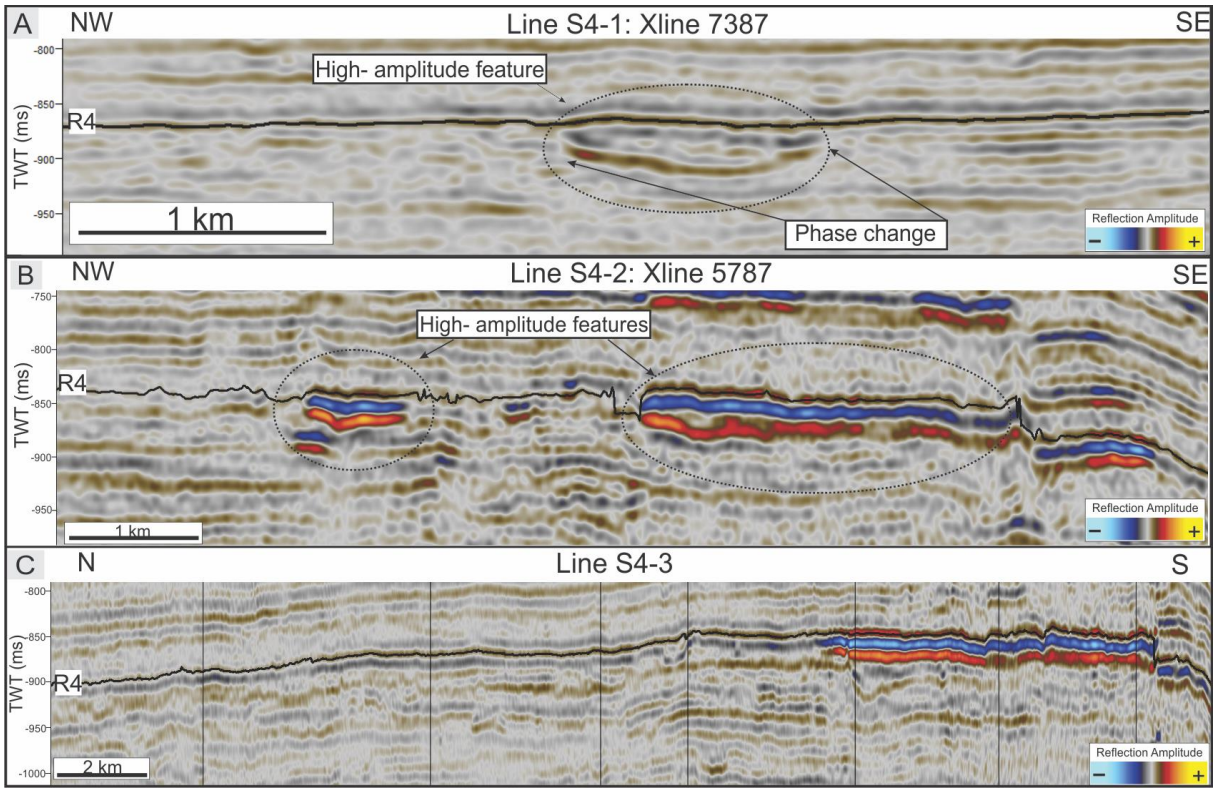

*Figure 4.15: Three different seismic sections showing the large high-amplitude feature seen in Figure 4.14. **A**: Seismic section from Xline 7387 showing the features vertical extent in the northern half. **B**: Seismic section from Xline 5787 showing both the main and side feature representing the southern part. **C**: Arbitrary seismic section following the main feature from the start in the north, to its southern end illustrating its regional extent, development and change.*

Interpretation: S4 contains one large feature, reaching almost throughout the entire data set, and the RMS-map clearly suggest that this is a large channel complex. The upper seismic section (Fig. 4.15A) show a clear erosive base with an infill structure above. This can be seen by the geometrical change at the bottom reflector compared with the surroundings, and the overlying slightly parallel, possibly phase reversed reflectors. Figure 4.15B visualizes the other part of the channel with a lower degree of depth/infill, but a much higher amplitude. Figure 4.15C indicate the same, with the reflector having a much larger amplitude in the southern area compared to the northern half.

A possible explanation to the change is that while the channel in the northern half have been erosive, the sediments have lost its transportation capacity in the southern half and because of this deposited much more sediments of a more shaly origin. This could also be a possible explanation to the smaller side channels. There are proven hydrocarbons within the channel complex. This can also explain the high amplitudes in the southern area, as gas decreases the acoustic impedance in the channel complex.

4.3.5 S5 - Unit 5

The upper unit S5 is limited by the R4 and Top Snadd reflectors. The unit is approximately 80 ms (twt) thick in average and partly eroded by the canyon-like features in the southern part of the study area. In the west, a couple of small high amplitude anomalies can be found in relation with the western small scale fault zone. The S5 unit can be described as uniform, with a possible overall western thinning trend (Fig.4.16). Other than the small features in the southern small scale fault zone, the unit have no large, significant amplitude features (Fig. 4.16). There is though possible to see some small, half-circular features in central parts of the study area, together with some longer, elongated features in the north.

Investigations of the seismic sections generally show higher amplitude values nearby and in relation with the southern small-scale fault zone. On a general basis, the seismic reflectors seem to be of higher values and more continuous in the upper compared to the lower part of S5.

A closer look at the top 50 ms of the formation/unit (Fig. 4.17) reveal more details of the features mentioned. The low to middle part of S5 contain a number of small, elongated features up to 10 km long (Fig. 4.17). The size and orientation of the features variate. Figure 4.17B highlights the small, crescent shaped features found between 30-50 ms below the Top Snadd reflector. Their overall shape are similar to the ones found in S3, but there are also clear differences considering the much more individual orientation and no internal sub-parallel lineations.

While the features are found in the middle part of the unit, the upper part seem to be largely uniform, with little to no irregular high-amplitude occurrences (Fig. 4.16C, 4.17C).

The gamma ray log of S5 indicate medium-high values (Fig. 4.4). The lower part of the unit have upwards decreasing log-values, while the upper half show an increase. The measurements are characterized as overall stable, but the log has slightly less variations in the upper part compared to the lower one.

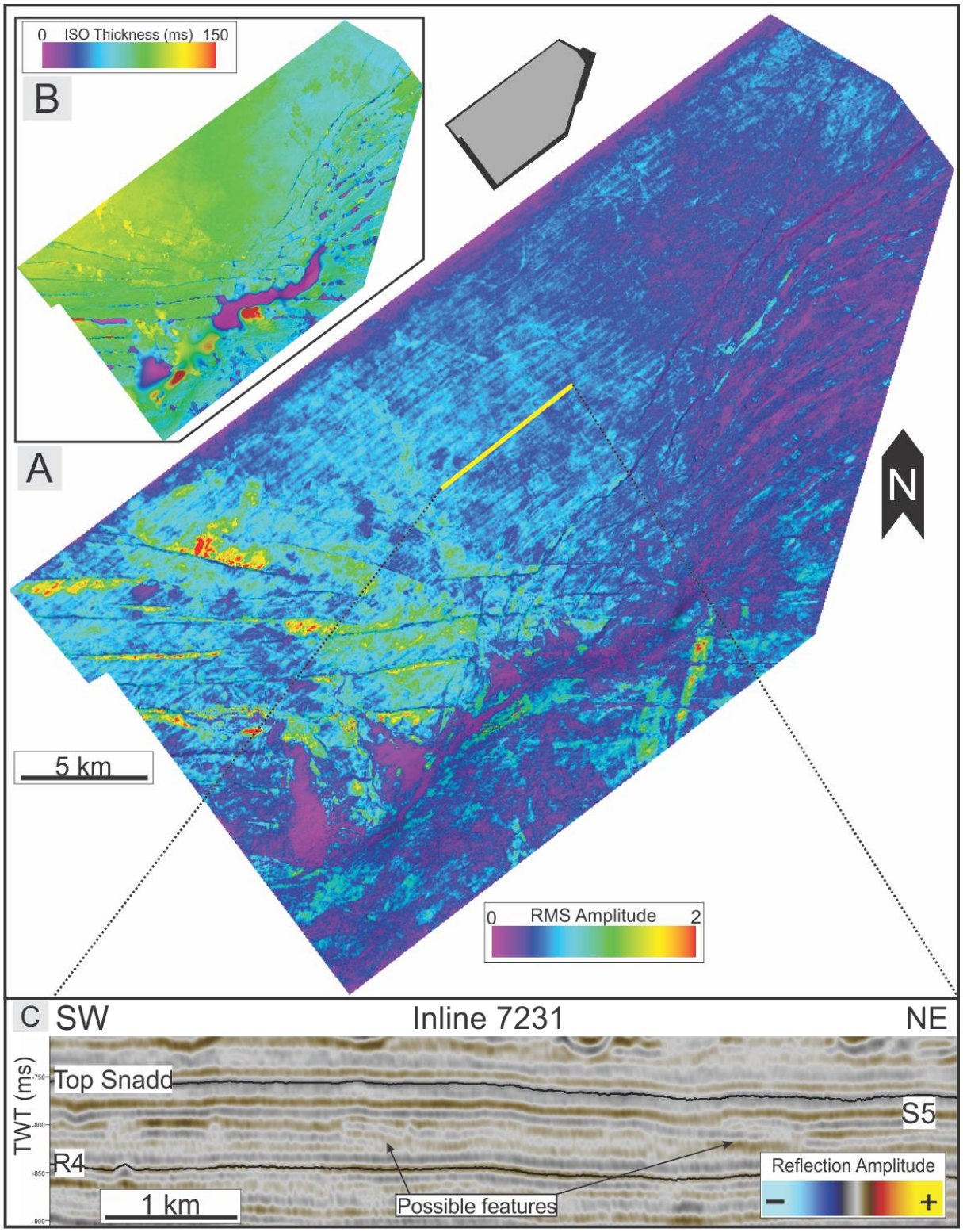

*Figure 4.16: **A**: RMS-map of the total seismic unit S5. **B**: Isochron time thickness map of the seismic unit S5. **C**: Seismic section at Inline 7231 indicating the S5 unit with possible features shown in Figure 4.17B.*

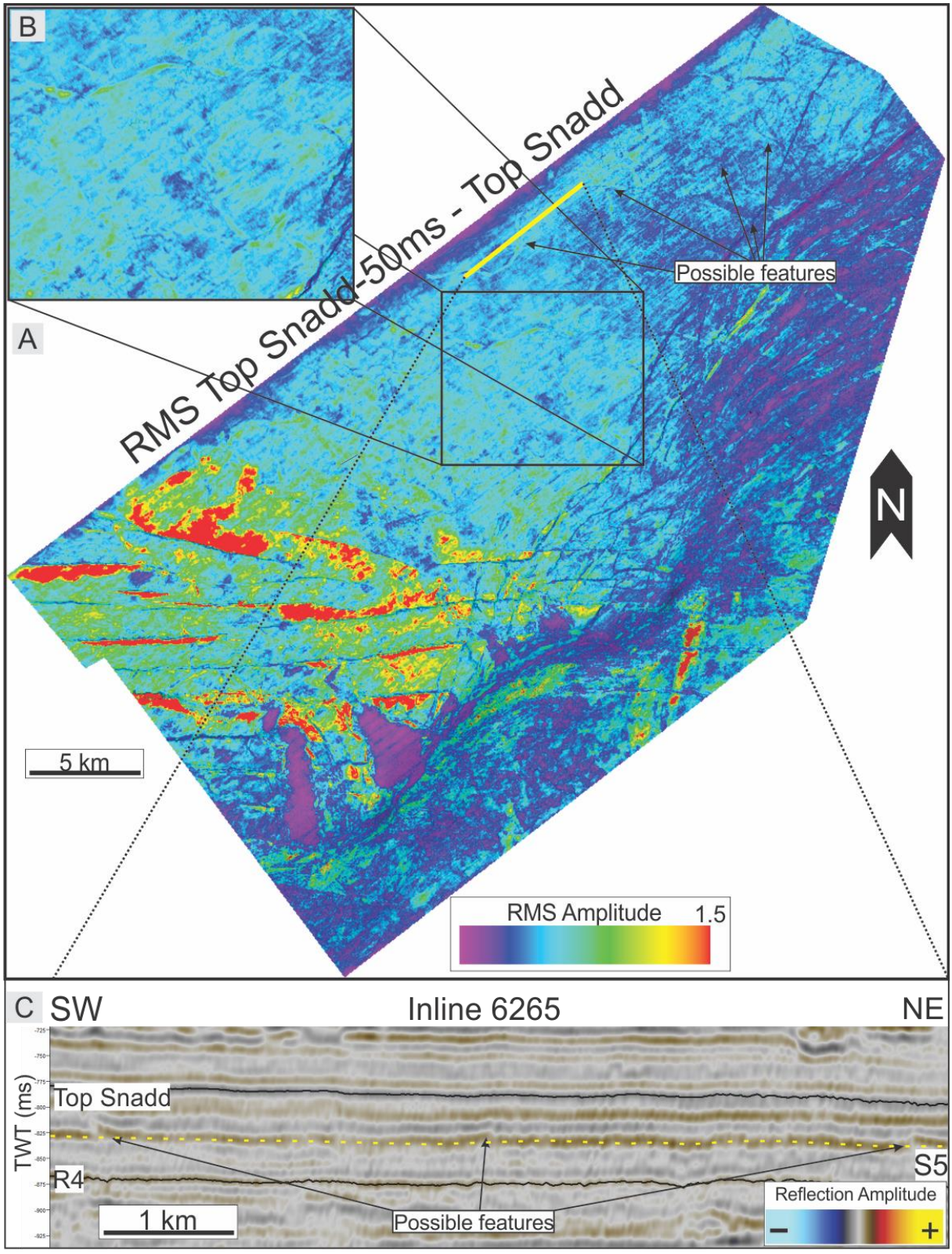

*Figure 4.17: **A**: RMS map generated from the volume between zero to 50 ms below the Top Snadd reflector. **B**: Zoom in on some of the smaller features found in A. **C**: Seismic section highlighting one of the possible features found in A. The map is extracted from the volume between the yellow dotted line and the Top Snadd reflector.*

Interpretation: The lower part of S5 is generally difficult to interpret with its discontinuous, transparent reflectors. The lower to middle part of the unit include some smaller features, and is thereby interpreted to be small channels in a coastal plain environment.

Above, a series of smaller crescent shaped features can be observed (Fig. 4.17A,B, Fig. 4.16C). With a NW-SE orientation the features is interpreted to be of a sandy, aeolian origin, deposited in a coastal environment, near the shoreface.

The uniform upper part of the unit with no large amplitude values, highly suggests that it has been deposited during a time and environment with low variations. An environment capable of this is most likely of marine origin. The high amplitudes in the southern area seem to be highly connected to the southern small scale fault zone. The high amplitudes around the faults are probably generated by fluid accumulation around Top Snadd. With an impermeable layer above, the fluids seem to accumulate in the upper part of the S5 region.

5. Discussion

5.1 Depositional environments of the Snadd Formation

The depositional environment is interpreted based on the seismic investigations and well log data presented in the previous chapter. The results will primarily be compared to earlier studies by Smelror et al., (2009), Glørstad-Clark et al., (2010), and Klausen et al., (2015).

5.1.1 The S1 unit

The relative uniform thickness of the S1 unit suggests that deposition may have taken place within a tectonically stable setting. The transparent internal reflections configuration (Fig. 4.5), the lack of any depositional features on the RMS maps, and the high gamma ray response are all together supportive of deposition within a marine environment.

The seismic investigations have revealed a consistent sedimentary unit with relatively low amplitude, discontinuous, transparent reflectors. The discontinuity of the reflectors makes it hard to interpret the reflector geometry, but a slight dip towards the west of the total package (Fig. 4.3 E,F) opens the possibility of the unit being deposited on a marine slope. The depositional environment does still seem unlikely, due to the absence of clinoforms (Chapter 1.4.1).

Another possible solution is that the depositions is of a bit shallower origin, a marine shelf environment (Chapter 1.4.2). This is supported by the fact that the unit has no highlighting clinoforms or toplap structures. The internal reflectors are somewhat untypical for a shallow marine environment, being discontinuous with a medium to low amplitude. Still, the reflector geometry makes this the most probable solution (Fig. 5.1).

The interpretation corresponds to earlier studies (Smelror et al., 2009; Glørstad-Clark et al., 2010; Klausen et al., 2015) concluding that the S1 unit is of marine origin. Klausen et al., 2015 suggests that the lower part of S1 is deposited in a marine slope environment, a interpretation not supported in this study due to the absence of clinoform structures throughout the unit.

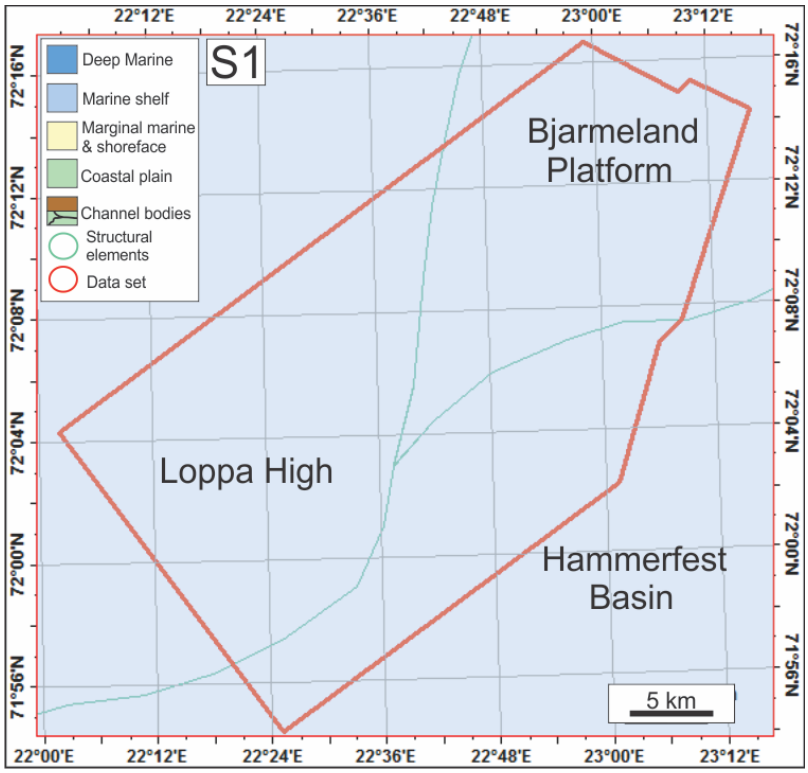

Figure 5.1: Paleogeographic map of the study area during deposition of unit S1.

5.1.2 The S2 unit

The S2 unit represent a unit with much larger variations than the underlying S1 both laterally and vertically, interpreted to represent distinct changes in the in the depositional environment. Inspections of the seismic sections show a difference in reflection amplitude and continuity between the lower and upper section, suggesting a change in the depositional environment at about 100 ms above the R1 reflector (Fig. 4.6, 4.8). Combining this with the trend change in the gamma ray, with much larger log variations in the upper section, this could possibly be a better mark for a change in the depositional environment than the actual R1 interpreted reflector. This change can be spotted at approximately 1700 meters depth in the well (Fig. 5.2, Fig. 5.6).

The lower feature found is situated about 50 ms above the R1 reflector, possibly correlated with the low values found in the gamma ray log around 1800 meters depth (Fig. 4.7A, 4.8A, 4.4). The feature is influenced by the small scale fault zone, making it harder to fully interpret. Though, the shape and extent of the feature suggests that it is more likely to be of aeolian than fluvial origin. Moving from a marine shelf environment,

the structure is interpreted to be a beach ridge deposited in an shoreface environment (Fig. 5.6).

The upper half of S2 include multiple features that all seem to be of fluvial origin (Fig. 4.8). This interpretation is based on investigations of the seismic sections, with an erosive base and possible infill. Thus, it seems likely to assume that while the lower part of S2 seems to be of marine origin, as S1, the area have undergone a marine regression during S2 from marine, through marginal marine, ending up at a coastal plain environment with small channel features (Fig. 5.2).

From the seismic sections it is though hard to see a clear marginal marine facies within the unit, but it is clear that we have a transition from marine shelf to coastal environment. The lack of a clear marginal marine environment within the section, could imply a sudden marine regression during the time of deposition (Fig. 5.2, Fig. 5.6).

The marine regression interpreted during early Carnian (middle S2) is widely acknowledged and well documented (Smelror et al., 2009; Glørstad-Clark et al., 2010; Klausen et al., 2015). The observations made in this study correlate with Klausen et al., (2015), suggesting a smaller marine regression followed by a marine transgression during lower S2. Earlier studies (Glørstad-Clark et al., 2010; Klausen et al., 2015) have interpreted a flooding surface during middle S2 (R1+100 ms), just below the large marine regression. Amplitude changes and gamma log values suggest that this probably is a better unit boundary than the interpreted R1 used in this study.

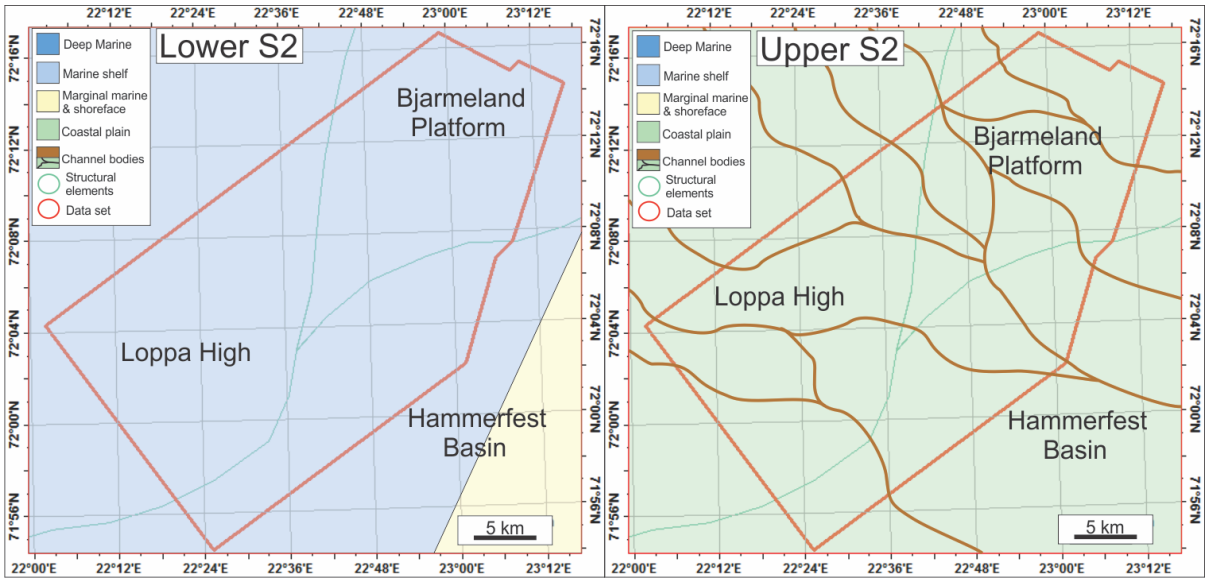

Figure 5.2: Paleogeographic map of the study area during deposition of lower and upper S2.

5.1.3 The S3 unit

Reflector R2 represent a clear change in reflector amplitude with higher values and a higher continuity. Supported by seismic analysis (Fig. 4.8B & 4.11A) the reflector is interpreted to be a flooding surface, marking a change from the coastal plain facies below to a marine shelf environment (Fig. 5.3 & 5.6). Above R2, the reflectors are of medium strength with variating continuity, quite similar to the upper part of S2. Differing from the upper S2, closer seismic analysis (RMS extraction) shows no depositional features within the lower 50 ms of the unit. This clearly points in the direction of a marine environment. The gamma ray log somewhat supports this with its medium to high values (although the log is not as stable as in S1 and the lower part of S2).

About 50 ms above R2 lies the lower of two high amplitude reflectors (Fig. 4.11) interpreted to be beach ridges and barchan dunes. The reflector shows no erosive signs suggesting a non-fluvial origin, while the low values of the gamma ray log indicate sandy conditions. These aeolian dunes are suggestive of a continental depositional environment, and hence, a change from a shallow marine to a coastal environment (Fig. 5.3 & 5.6). The large parallel features probably represents beach ridge sets, representing the shore, with land to the southeast and the shelf to the northwest (Chapter 1.4.3).

The section right above the previous seismic event show no signs of depositional features, before moving up to another large, straight feature interpreted to be another beach ridge with the same orientation (Fig. 4.11B). In comparison, the upper beach ridge has a much stronger amplitude, and is not found in relationship with other features. It is important to notice that the gamma ray log show its lowest recorded values within the Snadd Formation (Fig. 4.4). This further supports the theory of a coastal, sandy environment (Fig. 5.3 & 5.6).

The upper part of the section, above the large features, is similar to the lower part of S3, with medium amplitudes and continuity. As the lower part, the upper one also show no signs of high amplitude features, suggesting a marine regression back to a marine environment (Fig. 5.3 & 5.6). The gamma ray log has low variations in the upper part of the unit, supporting the interpretation (Fig. 4.4). The log also, during this part, have an overall gamma ray increase before a large change during R3.

The R2 reflector corresponds with the Intra Early Carnian MFS described in Klausen et al., (2015), and S3 with the C2 unit. The interpretation by Klausen et al., (2015) indicate the same marine regression during early stages, with the shoreface crossing the study area during regression maximum in middle S3 and transgression during late S3.

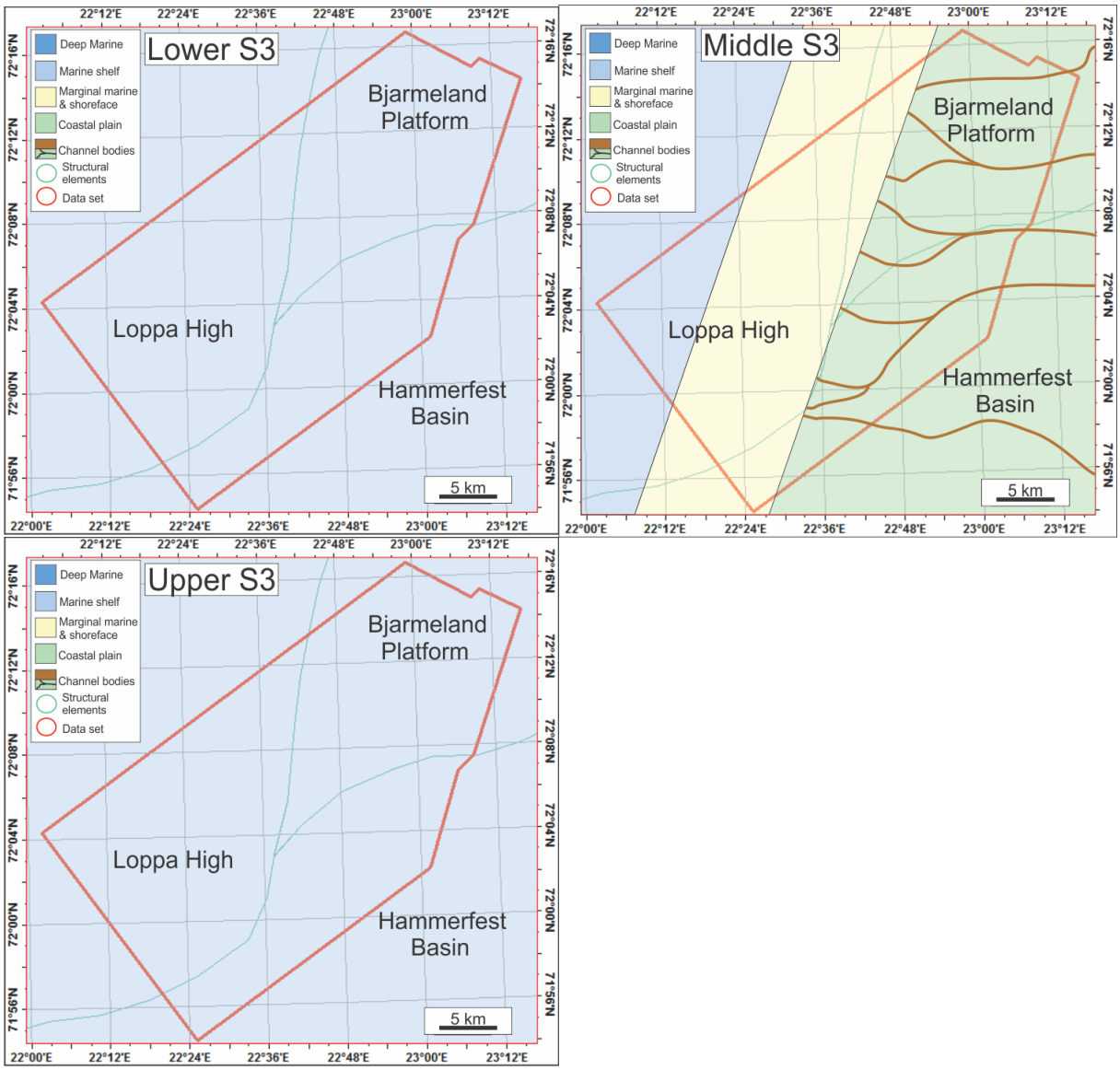

Figure 5.3 Paleogeographic map of the study area during deposition of lower, middle and upper S3.

5.1.4 The S4 unit

The R3 reflector marks a flooding surface, and based on the log increase in GR, a sudden change in the deposited sediment composition (Fig. 4.4). This large change suggests that this could be characterized as a second-order change following terminology from earlier research (Glørstad-Clark et al., 2010; Klausen et al., 2015), while the other can be characterized as a change of third order. The S4 unit is a unit of variety, with the reflectors ranging from strong and continuous to weak and discontinuous. After what seems to be a little transition period just above R3, the section seems to include large amounts of smaller channels moving upwards in the seismic (Fig. 4.13). All the channels are similar considering shape and size, some of them connected in series. Their erosive base and infill strongly suggests a coastal plain environment. As previously seen during S2, there is no sign of a marginal marine environment. This suggests a sudden marine transgression, with the depositional environment changing rapidly from a marine shelf to a coastal plain environment (Fig. 5.4 & 5.6).

The trend continues throughout the unit, but just below R4 there is a channel sandstone body much larger than the others found in the dataset (Fig. 4.14). Studies of the seismic sections show clear changes within it, with higher amplitudes and shorter depths in the western part compared to the east(Fig. 4.15). From this, it seems to be a logical solution that the channel had its movement from northeast to southwest. This correlates with the overall trend in the area (Klausen et al., 2015). The direction of movement could also be a possible explanation to the changing amplitude between the west and the east, with more sediments being deposited in the western area. The channel is proven to contain hydrocarbons, both in the form of oil and gas (NPD, 2016). Gas has a massive influence on the reflection amplitude, and is probably the largest explanation to the large amplitude difference between the eastern and western part.

The late Carnian is characterized by an extensive westwards progradation of the coastal depositional environment (Smelror et al., 2009). The study corresponds to this with a coastal plain environment throughout the section, and with the largest channel bodies observed in upper S4. The R3 reflector from this study is located a bit higher than the Intra Carnian MFS interpreted by Klausen et al., (2015), and seems to locate the log

change, suggesting that it splits the unit during the change from marine to a coastal plain environment.

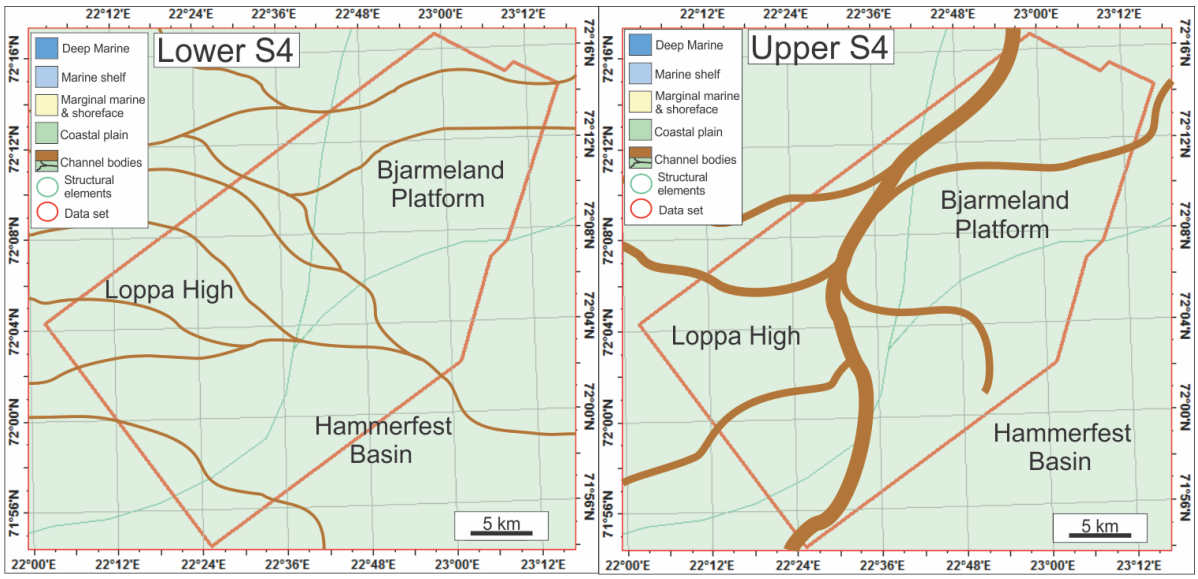

Figure 5.4: Paleogeographic map of the study area during deposition of lower and upper S4.

5.1.5 The S5 unit

S5 represents the upper part of the Snadd Formation, and contain a variety of reflectors ranging from continuous with high amplitudes to discontinuous and transparent (Fig. 4.16 & 4.17). The lower part of the section include smaller channel features (Fig. 4.17), deposited in a coastal plain environment. During middle S5 a number of crescent shaped, slightly tilted reflectors can be observed, interpreted to be aeolian dunes (Fig. 4.16C & Fig. 4.17B). This suggests a change from a coastal plain to a sandy coastal environment (Fig. 5.5 & 5.6). In the upper S5 section, it is interpreted to be a marine transgression, moving to a marine shelf environment (Fig. 5.5 & 5.6). This interpretation is based on the reflection configuration (Fig. 4.16C), the lack of depositional features and the slight GR increase (Fig. 4.4). This implies a change from a coastal plain to a marine environment within the section. This interpretation agrees with earlier studies of the Top Snadd being a flooding surface (Mørk, 1999).

The high amplitudes found within the unit is located in the western part, and seems to be in relation to the southern small-scale fault zone (Fig. 4.2 & 4.17). Bearing in mind that the area is hydrocarbon proven, it is a fact that faults tend to act as a migration path

through impermeable layers. If the layer above the Top Snadd is impermeable (supported by the gamma ray log), the gas will migrate into the Top Snadd layer and contribute to its high amplitudes.

The interpretation correlates with earlier studies concluding with an overall marine transgression during S5, moving from a large coastal plain to a marine shelf environment (Mørk, 1999; Smelror et al., 2009; Glørstad-Clark et al., 2010; Klausen et al., 2015).

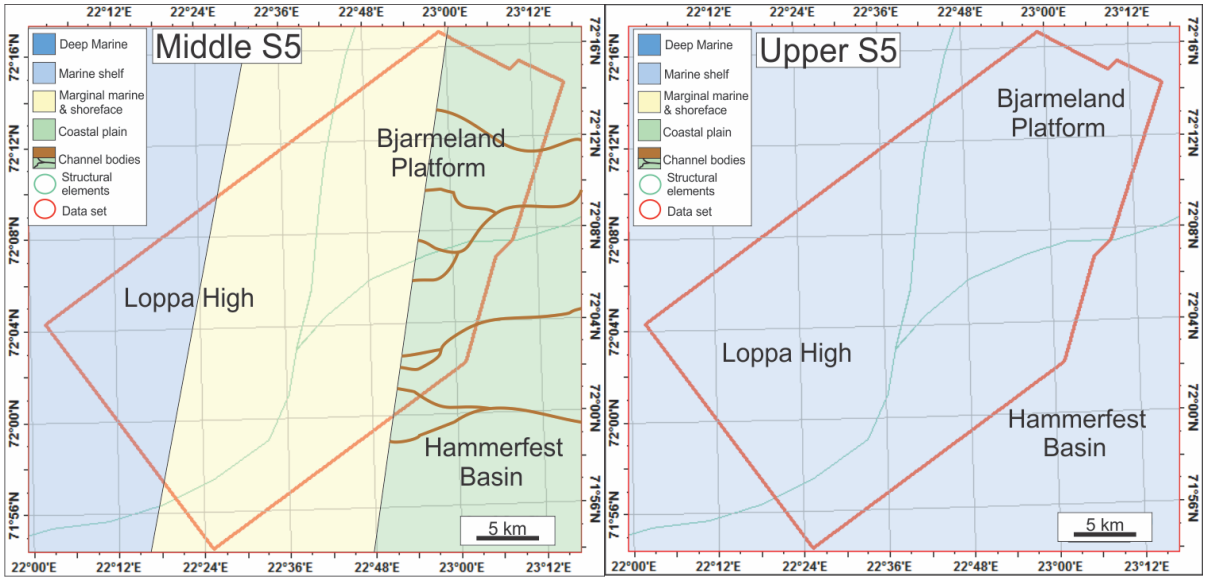

Figure 5.5: Paleogeographic map of the study area during deposition of middle and upper S5.

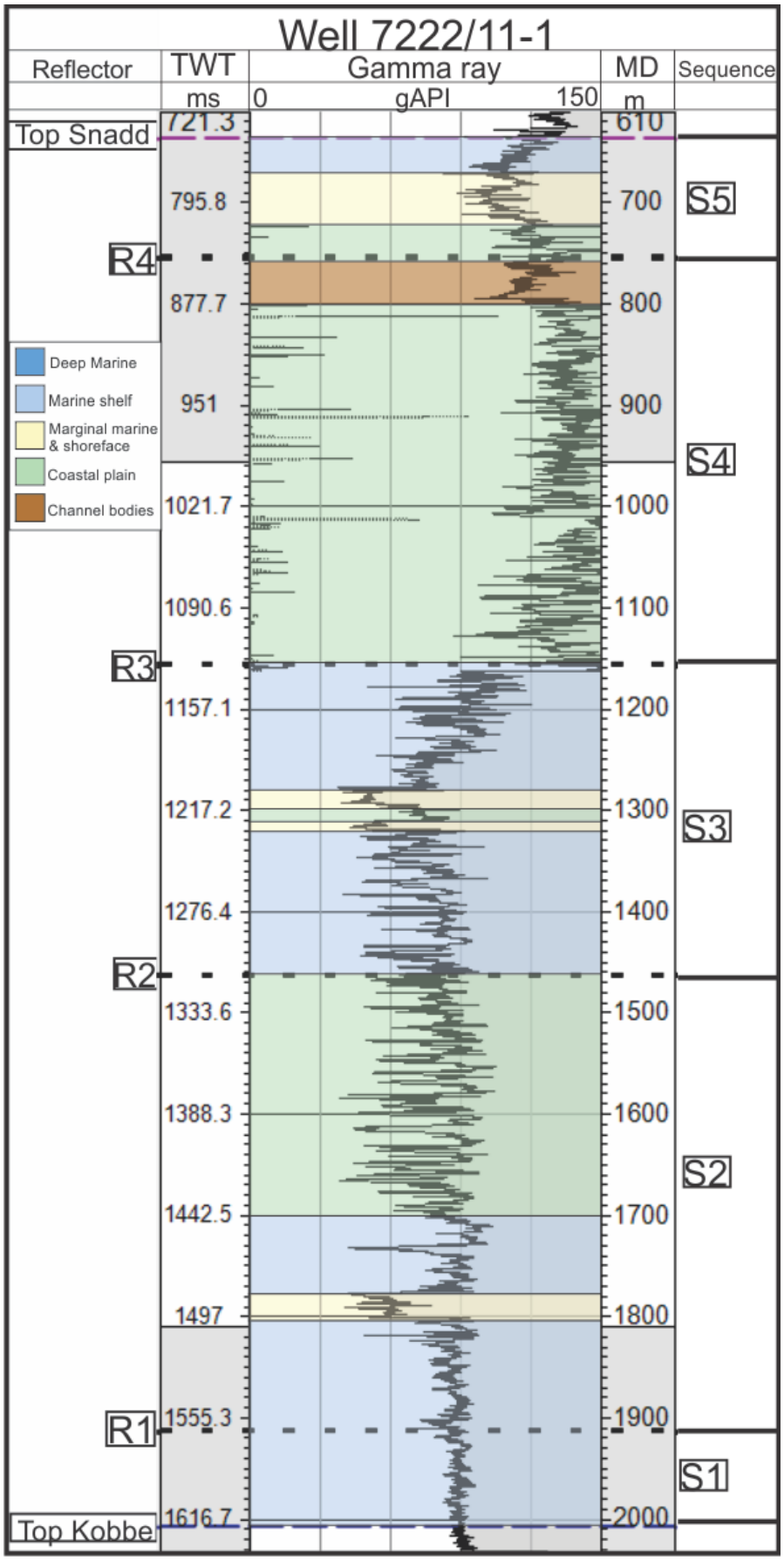

Figure 5.6: Well log including the interpreted environmental changes in the Snadd Formation.

5.2 A revised seismic stratigraphy for the Snadd Formation

The Snadd Formation as a part of the Upper Triassic stratigraphy in the Barents Sea has been a subject to recent studies, with different methodologies resulting in different interpretations (Glørstad-Clark et al., 2010, 2011; Klausen et al., 2015). Similarities and differences between the studies is summarized in Figure 5.7, along with the Svalbard correlating formations from Mørk et al., (1999). Glørstad-Clark et al., (2010) divided the Middle to Late Triassic into two second-order units, while Klausen et al., (2015) later splits the Snadd Formation into two (different) second-order units and six third-order subunits.

As for the previous research, this study divides the formation into two second-order units split by the Intra Carnian FS. The formation is further divided into five third-order units split by six flooding surfaces. Stratigraphically, the second-order boundary is located higher in the present study compared to Glørstad-Clark et al., (2010), which seem to have located the boundary in middle S2 at the change from marine to coastal settings (Fig. 4.8). The boundary in this study concludes similarly to the interpretation by Klausen et al., (2015).

The differences between the third-order units interpreted in this study and the results from Klausen et al., (2015) are small, but the units covers slightly different time periods. The biggest difference between the two results is found in the lower units (L1 versus S1), where L1 covers a larger volume compared to S1, enclosing the lower sandy event found during S2. Klausen et al., (2015) also suggests that C3 could be divided into two subunits (C3 and C4) (Fig. 5.7). This thesis has not observed a boundary within S4 supporting this suggestion.

The results from this study is based on data from a relatively small area of the southwestern Barents Sea. In order to test the stratigraphic results of the study further, future research should map the stratigraphic results regionally in the Barents Sea.

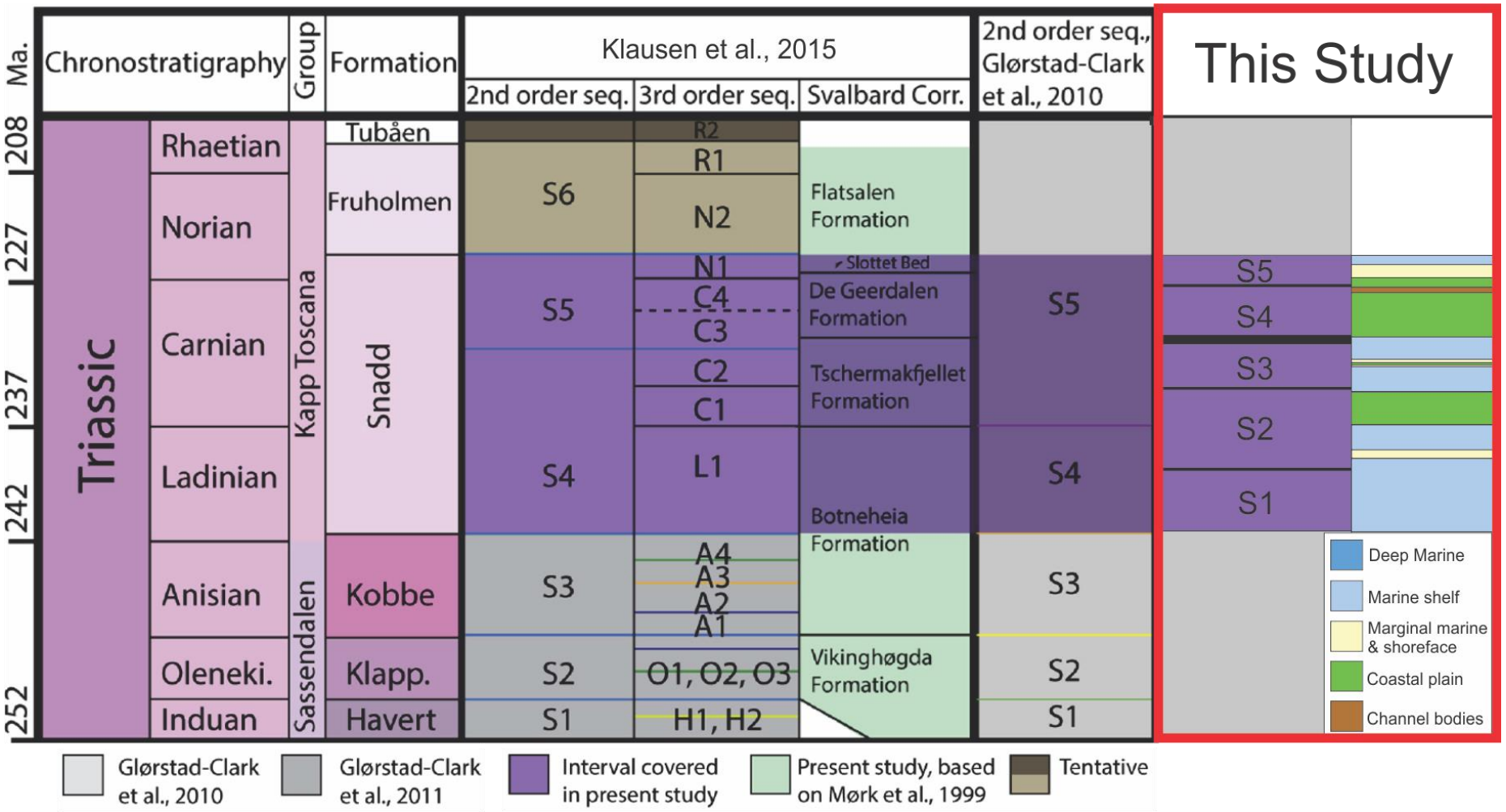

Figure 5.7: Comparison of units subdivisions compared with earlier studies with the interpreted changes within the depositional environment. Data from Glørstad-Clark et al., (2010) and Klausen et al., (2015). Figure modified from Klausen et al., (2015).

6. Summary & Conclusion

The Snadd Formation covers a time-period with multiple marine regressions and transgressions, with the depositional environment changing between a marine shelf and a coastal plain facies. The different changes is summarized below:

- Unit S1 was deposited in a marine shelf environment, with stable sedimentary depositions closed from outer erosional and depositional processes.
- Unit S2 include a change in the depositional environment during middle S2 from marine to a coastal plain, due to a marine regression. The upper sub-unit in S2 contain multiple small scale channel structures.
- Unit S3 is defined by a flooding surface base created by a marine transgression, moving back from a coastal plain- to a marine shelf environment. During middle S3 the environment changes from marine shelf to coastal/shoreface. This conclusion is due to the presence of both beach ridges and barchan dunes, together with a log confirmation of a sandy environment. During upper S3 a marine transgression again created a marine shelf environment.
- Unit S4 include a marine regression close to its base, changing the depositional environment from marine shelf to coastal plain. The environment is constant within the unit, with the largest channel structure of the data set observed near the top of S4.
- Unit S5 show smaller channel structures deposited in a coastal plain environment in its lower section. During middle S5 barchan dunes reveal an environmental change, moving into more coastal settings. During upper S5 a marine transgression floods the area, moving it back to a marine shelf environment.
- The results from this study is based on data from a relatively small area of the southwestern Barents Sea. In order to test the stratigraphic results of the study further, future research should map the stratigraphic results regionally in the Barents Sea.

7. References

Andreassen, K., 2009. *Marine Geophysics, Lecture notes for Geo-3123.* s.l.:University of Tromsø.

Badley, M. E., 1985. *Practical Seismic Interpretation.* Boston, MA: IHRDC Press.

Brown, A. R., 1999. *Interpretation of three-dimensional seismic data.* s.l.:American Association of Petroleum Geologists and the Society of Exploration Geophysicists..

Bugge, T., Elvebakk, G., Fanavoll, S., Mangerud, G., Smelror, M., Weiss, H.M., Gjelberg, J., Kristensen, S.E. & Nilsen, K., 2002. Shallow stratigraphic drilling applied in hydrocarbon exploration of the Nordkapp Basin, Barents Sea. *Mar. Pet. Geol.* 19, 13-37.

Bulat, J., 2005. Some considerations on the interpretation of seabed images based on commercial 3D seismic in the Faroe-Shetland Channel. *Basin Research,* Volume 17, pp. 21-42.

Bullimore, S., Larssen, G.B., Laursen, I., Sollid, K., Ashton, N. & Henriksen, S., 2004. Concepts in Predicting Lithology in Prograding Systems from High Resoltion Seismic Imaging: Examples from the Arctic Barents Sea. *University of Bergen*, Bergen, p. 44.

Dalland, A., Worsley, D. & Ofstad, K., 1988. A Lithostratigraphic Scheme for the Mesozoic and Cenozoic Succession Offshore Mid- and Northern Norway. *Direktoratet*, Stavanger.

Doré, A. G., 1995. Barents Sea Geology, Petroleum Resources and Commercial Potential. *Arctic,* Volume 48, pp. 207-221.

Faleide, J. I., Vågenes, E. & Gudlaugsson, S. T., 1993. Late Mesozoic-Cenozoic evolution of the south-western Barents Sea in a regional rift-shear tectonic setting. *Marine and Petroleum Geology,* Volume 10, pp. 186-214.

Faleide, J. I., Solheim, A., Fiedler, A., Hjelstuen, B. O., Andersen, E. S., & Vanneste, K. 1996. Late Cenozoic evolution of the western Barents Sea-Svalbard continental margin. *Global and Planetary Change,* 12, 53-74.

Gabrielsen, R. et al., 1990. Structural elements of the Norwegian continental shelf, Part I: The Barents Sea Region. *NPD-bulletin,* Volume 6.

Glørstad-Clark, E., Faleide, J., Lundschien, B. & Nystuen, J., 2010. Triassic seismic sequence stratigraphy and paleogeography of the western Barents Sea area. *Marine and Petroleum Geology,* Volume 27, pp. 1448-1475.

Glørstad-Clark, E., Birkeland, E.P., Nystuen, J.P., Faleide, J.I. & Midtkandal, I., 2011. Triassic platform-margin deltas in the western Barents Sea. *Mar. Pet. Geol.* 28, 1294-1314.

Gudlaugsson, S., Faleide, J., Johansen, S. & Breivik, A., 1998. Late Palaeozoic structural development of the South-western Barents Sea. *Marine and Petroleum Geology,* Volume 15, pp. 73-102.

Henriksen, E., Bjørnseth, H.M., Hals, T.K., Heide, T., Kiryukhina, T., Kløvjan, O.S., Larssen, G.B., Ryseth, A.E., Rønning, K., Sollid, K. & Stoupakova, A., 2011a. Uplift and erosion of the greater Barents Sea: impact on prospectivity and petroleum systems (Chapter 17). *Geological Society, London, Memoirs* 35, pp. 271-281.

Henriksen, E., Ryseth, A.E., Larssen, G.B., Heide, T., Rønning, K., Sollid, K. & Stoupakova, A.V., 2011b. Tectonostratigraphy of the greater Barents Sea: implications for petroleum systems (Chapter 10). *Geological Society, London, Memoirs* 35, pp. 163-195.

Johansen, S.E., Ostisky, B.K., Birkeland, Ø., Fedrovsky, Y.F., Martirosjan, V.N., Bruun Christensen, O., Cheredeev, S.I., Ignatenko, E.A. & Margulis, L.S., 1993. Hydrocarbon potential in the Barents Sea region: play distribution and potential. In: Vorren, T.O., Bergsager, E., Dahl-Stamnes, Ø.A., Holter, E., Johansen, B., Lie, E. & Lund, T.B. (Eds.)*, Arctic Geology and Petroleum Potential. Elsevier*, Amsterdam, pp. 273-320.

Klausen, T. G., Ryseth, A. F., Helland-Hansen, W., Gawthorpe, R. & Laursen, I., 2015. Regional development and sequence stratigraphy of the Middle to Late Triassic Snadd Formation, Norwegian Barents Sea. *Marine and Petroleum Geology,* Volume 62, pp. 102-122.

Laberg, J. S., Andreassen, K. & Vorren, T. O., 2012. Late Cenozoic erosion of the high-latitude southwestern Barents Sea shelf revisited. *Geological Society of America Bulletin,* vol. 124, 77-88.

Mørk, A., Elvebakk, G., 1999. Lithological description of subcropping Lower and Middle Triasic rocks from the Svalis Dome, Barents Sea*. Polar Res*. 18, 83-104.

Mørk, M. B. E., 1999. Compositional Variations and Provenance of Triassic Sandstones From the Barents Shelf. *Journal of Sedimentary Research,* 69(3), pp. 690-710.

NPD. 2016. Norwegian Petroleum Directorate Factpages [Online]. Available: http://factpages.npd.no/factpages/Default.aspx?culture=no (May 2016)

Riis, F., Lundschien, B.A., Høy, T., Mørk, A. & Mørk, M.B.E., 2008. Evolution of the Triassic shelf in the northern Barents Sea region. *Polar Res.* 27, 318-338.

Schlumberger, 2010. *Interpreter's Guide to Seismic Attributes.* Huston: Schlumberger.

Sheriff, R., 1985. Aspects of Seismic Resolution. *Seismic Stratigraphy II: American Association of Petroleum Geologists, Memoir,* Volume 39, pp. 1-10.

Sheriff, R.E. 2006. Encyclopedic dictionaryof exploration geophysics, 4th edition. *Society of Exploration Geophysicists, Tulsa.*

Skjold, L.J., van Veen, P.M., Kristensen, S.-E. & Rasmussen, A.R., 1998. Triassic sequence stratigraphy of the southwestern Barents Sea. In: de Graciansky, P.-C., Hardenbol, J., Jacquin, T. & Vail, P.J. (Eds.), *Mesozoic and Cenozoic Sequence* T.G. Klausen et al. / Marine and Petroleum Geology 62 (2015) 102-122 *Stratigraphy of European Basins.* Society for Sedimentary Geology (SEPM), Tulsa, pp. 651-666.

Smelror, M., Petrov, O., Larssen, G. B. & Werner, S., 2009. *Geological History of the Barents Sea.* Trondheim: Geological Survey of Norway.

Sollid, K., Ashton, N., Gytri, S. R., Henriksen, L.B., Larssen, G.B., Laursen, I. & Rønning, K., 2004. Triassic Paleoenvironments, Southwestern Barens Sea. New Plays emerging from 3D seismic facies mapping. *NGF Abstract and Proceedings*, no. 2, 168-170.

van Veen, P.M., Skjold, L.J., Kristensen, S.E., Rasmussen, A., Gjelberg, J. & Stølan, T., 1993. Triassic sequence stratigraphy in the Barents Sea. In: Vorren, T.O., Bergsager, E., Dahl-Stamnes, Ø.A., Holter, E., Johansen, B., Lie, E. & Lund, T.B. (Eds.), *Arctic Geology and Petroleum Potential*, NPF Special Publication, second ed. Elsevier, Amsterdam, pp. 515-538.

Vorren, T.O., Richardsen, G., Knutsen, S. M. & Henriksen, E. 1991. Cenozoic erosion and sedimentation in the western Barents Sea. *Marine and Petroleum Geology,* 8, 317-340

Worsley, D., 2008. The post-Caledonian development of Svalbard and the western Barents Sea. *Polar Research,* Volume 27, pp. 298-317.